Inorganic Chemistry
Cite This: Inorg. Chem. XXXX, XXX, XXX–XXX
Article
pubs.acs.org/IC

Intramolecular $\pi-\pi$ Interactions with a Chiral Auxiliary Ligand Control Diastereoselectivity in a Cyclometalated Ir(III) Complex

Daniel G. Congrave,[†] Andrei S. Batsanov,[†] Mingxu Du,[‡] Yu Liu,*[,‡] Dongxia Zhu,*[,§] and Martin R. Bryce*[,†]

[†]Department of Chemistry, Durham University, South Road, Durham DH1 3LE, U.K.

[‡]State Key Laboratory of Supramolecular Structure and Materials, College of Chemistry, Jilin University, Changchun 130012, People's Republic of China

[§]Key Laboratory of Nanobiosensing and Nanobioanalysis at Universities of Jilin Province, Department of Chemistry, Northeast Normal University, 5268 Renmin Street, Changchun, Jilin 130024, People's Republic of China

Supporting Information

ABSTRACT: The application of a chiral auxiliary ligand to control the diastereoselectivity in the synthesis of a cyclometalated iridium(III) complex is presented. The diastereomeric iridium(III) complexes **1a** and **1b** are reported, in which a phenoxyoxazoline auxiliary ligand incorporates a chiral center functionalized with a pendant pentafluorophenyl group. The diastereomers were readily separated, and their structural, electrochemical and photophysical properties are discussed. Solution-state NMR data and X-ray crystal structures establish that the pentafluorophenyl group engages in intramolecular $\pi-\pi$ interactions. The X-ray analysis reveals that the two diastereomers display very different modes of intramolecular stacking. The variable-temperature ^{19}F NMR data indicate that rotation of the pendant pentafluorophenyl rings in **1b** and **1a** is a temperature-dependent process and that there is a smaller energy barrier to rotation in **1b** in comparison to **1a**. This correlates with variable-temperature photoluminescence data, which show that upon heating the integrated emission intensity is reduced substantially more for **1b** than for **1a**, which is ascribed to the enhanced rotation in **1b**, providing a more easily populated nonradiative pathway in comparison to **1a**. These experimental data are supported by computational calculations. Phosphorescent organic light-emitting devices (PhOLEDs) using **1a** as the dopant complex give blue-green emission with a high maximum external quantum efficiency (EQE_{max}) of 25.8% (at ca. 270 cd m^{-2}) and with a low efficiency roll-off to 24.9% at 1000 cd m^{-2}. Our results extend the scope of ligand design for cyclometalated iridium complexes which possess interesting structural and emission properties.

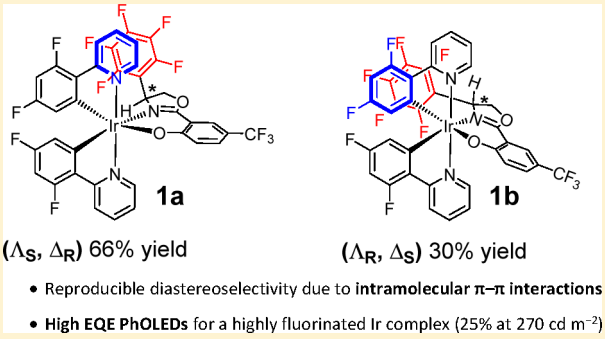

INTRODUCTION

Iridium(III) complexes have been widely studied in applications[1,2] such as photocatalysis,[3] biological labeling,[4] and sensing[5] and as emitters in highly efficient phosphorescent organic light-emitting devices (PhOLEDs).[6−12] They possess a range of advantageous properties such as high luminescence quantum efficiency (Φ), microsecond-scale phosphorescence lifetime (τ), and good electrochemical stability, while their metal−ligand based photochemistry has enabled their emission color to be tuned across the entire visible spectrum through appropriate synthetic modifications.[13−15]

Notably, highly phosphorescent heteroleptic complexes have received significant interest because they can be synthesized under milder conditions in comparison to *fac*-homoleptic complexes, allowing a wider scope for structural variation.[16−19] They typically feature two cyclometalating C^N chelates, which function as luminophores, alongside a third auxiliary ligand that is not directly involved in the excited state (ancillary) but instead can influence emission color and orbital mixing through tuning of the energy of the Ir d orbitals.[20−26]

An interesting way to alter this classic system is through the incorporation of phenoxyazole-based ligands as the third chelate, which provides unusual complexes where the auxiliary ligands feature significant frontier orbital contribution. Several highly emissive derivatives have been reported by our group and others, including application in efficient PhOLEDs.[27−30] In particular, we have established that synthetic modification of such auxiliary ligands can be used to control emission color through tuning either the frontier orbital energies or the emission bandwidth.[28,29]

Received: July 19, 2018

DOI: 10.1021/acs.inorgchem.8b02034
Inorg. Chem. XXXX, XXX, XXX–XXX

Noncovalent interactions are another promising tool for altering the photophysical properties of luminophores.[31,32] Their incorporation can offer synthetic control while avoiding the difficulties associated with the construction of covalent bonds. For example, in a sky blue bis[2-(4,6-difluorophenyl)-pyridinato-C^2,N](picolinato)iridium(III) (FIrpic) based system, a comparison of hydroxy- and methoxy-substituted derivatives unequivocally established that intramolecular hydrogen bonding decreased the nonradiative decay rate (k_{nr}) by 1 order of magnitude and increased PhOLED operating time by over 50%.[31]

Intramolecular $\pi-\pi$ stacking has been incorporated into a few specific iridium complexes[33−38] and has been shown to improve the operational stability of light-emitting electrochemical cells (LEECs).[33] In addition, intramolecular $\pi-\pi$ interactions can rigidify complexes, thereby enhancing their photoluminescence quantum yields (PLQYs)[35,38] when perfluoroaryl groups are included to augment stacking.[39−41] However, it is difficult to determine the exact consequences of intramolecular stacking, as its presence/absence inevitably alters secondary electronic and/or steric factors.[39,42−44]

In this study we intended to circumvent this issue by studying the new diastereomeric complexes **1a** and **1b** (Figure 1).

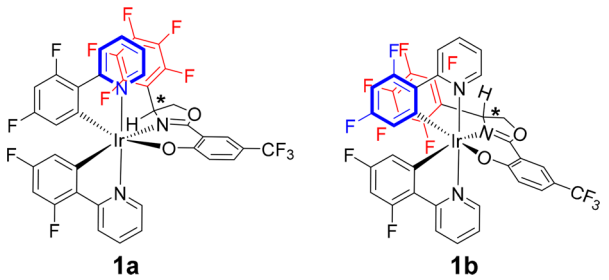

Figure 1. Structures of diastereomeric complexes **1a** and **1b** with their 3D configurations. The colored rings engage in intramolecular $\pi-\pi$ interactions.

Their phenoxyoxazoline auxiliary ligands (**6**; Figure 2) incorporate a chiral center functionalized with a pendant pentafluorophenyl group. As **1a** and **1b** are diastereomeric, they are expected to have nearly identical electronic properties. However, the pentafluorophenyl ring was expected to display different stacking modes in **1a** and **1b**.[30,45] Consequently, it was anticipated that any significant differences in the photophysical properties of **1a** and **1b** would be specifically related to the nature of their intramolecular $\pi-\pi$ interactions.

The diastereomers **1a** and **1b** were separated, and their structural, electrochemical, and photophysical properties are reported. Experimental data are supported by a density functional theory (DFT) study. In particular, variable-temperature (VT) ^{19}F NMR and photoluminescence (PL) measurements provide insights into the influence of the intramolecular $\pi-\pi$ interactions on the solution photophysical properties of **1a** and **1b**. Vacuum-processed PhOLEDs doped with **1a** as the emitter demonstrate notably good performance for a perfluoroaryl-functionalized Ir complex.

RESULTS AND DISCUSSION

Synthesis. Monari, Bandini, Ceroni, and co-workers previously demonstrated that chiral phenoxyoxazoline auxiliary ligands functionalized with pendant phenyl rings afford highly

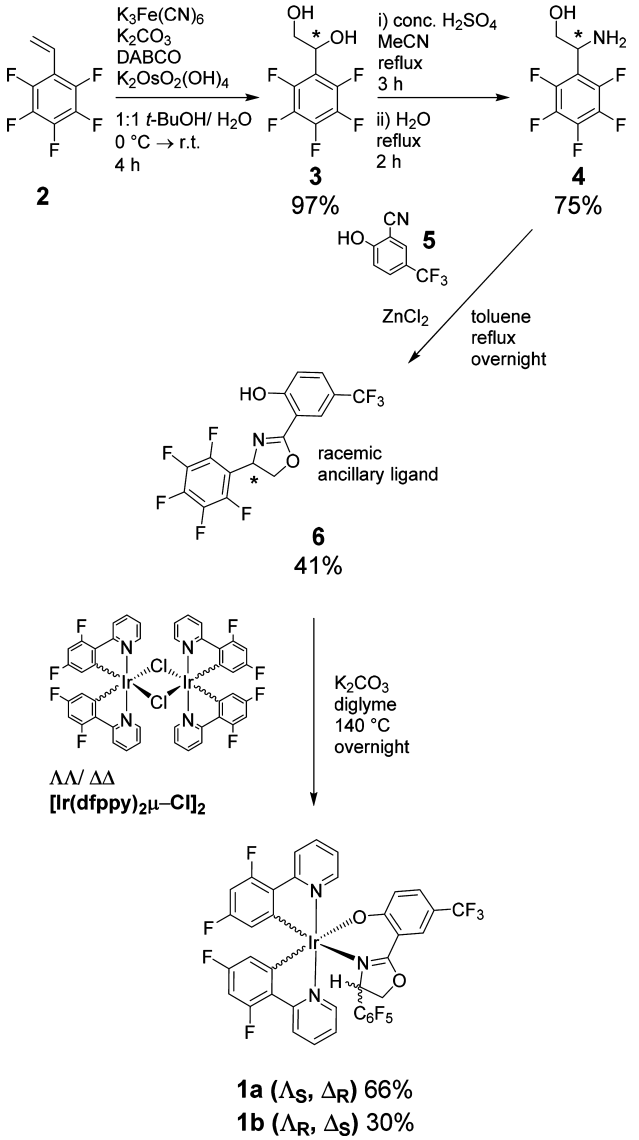

Figure 2. Syntheses of the chiral auxiliary ligand **6** and the diastereomeric complexes **1a** and **1b**.

emissive Ir complexes, the diastereomers of which were separated.[30] Weak intramolecular $\pi-\pi$ interactions were observed between cyclometalating pyridyl and pendant phenyl moieties in the Λ_S, Δ_R diastereomers (stereochemistry analogous to **1a**) by X-ray crystallography, with centroid−centroid distances of 3.65−4.31 Å. Inspired by this work, we devised the chiral auxiliary ligand **6** with a pendant pentafluorophenyl group to enhance intramolecular $\pi-\pi$ interactions.[39−41] 2-(2,4-Difluorophenyl)pyridine (dfppy) cyclometalating ligands were selected because they afforded higher PLQYs in comparison to 2-(phenyl)pyridine (ppy) in previous work.[30] In addition, when they are implemented alongside the CF_3 group on the phenoxy moiety of the auxiliary ligand, these ligands would allow the study of intramolecular $\pi-\pi$ interactions in a system with an emission energy higher than that of Ir(ppy)$_3$.[29]

The synthetic scheme for the ligand **6** and complexes **1a** and **1b** is shown in Figure 2. The racemic aminoethanol derivative **4** was synthesized via the dihydroxylation of pentafluorostyrene (**2**) followed by the Ritter rearrangement of **3**.[46] Subsequent $ZnCl_2$-catalyzed condensation with the commercial

DOI: 10.1021/acs.inorgchem.8b02034
Inorg. Chem. XXXX, XXX, XXX−XXX

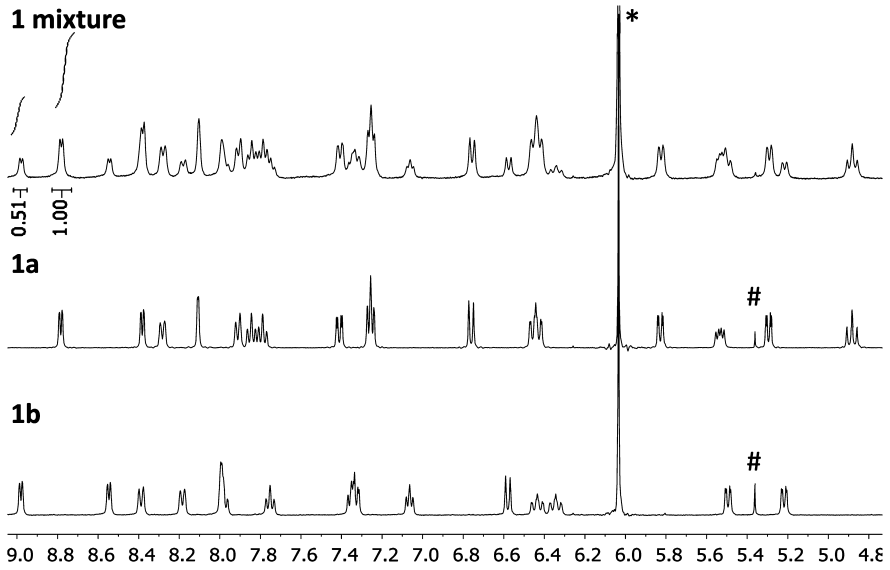

Figure 3. Aromatic regions of the ^{1}H NMR spectra of crude **1** and the resolved diastereomers **1a** and **1b** in d_2-1,1,2,2-tetrachloroethane to highlight the ca. 2:1 diastereomeric ratio. Legend: (*) residual d_1,H$_1$-1,1,2,2-tetrachloroethane in the NMR solvent; (#) CH_2Cl_2. Chemical shifts are given in ppm.

benzonitrile derivative **5** afforded racemic **6** in 41% yield. Reaction of **6** with the racemic dimeric complex $[Ir(dfppy)_2(\mu\text{-}Cl)]_2$ resulted in near-quantitative conversion to the diastereomers **1a** and **1b**, which were each formed as a racemic pair of enantiomers. Anhydrous diglyme was selected as solvent to avoid any nucleophilic aromatic substitution side reactions on the perfluoroaryl ring of **6**.

The diastereomers **1a** and **1b** were easily separated via column chromatography and isolated in yields of 66% and 30%, respectively. Analysis of the crude evaporated reaction mixture by ^{1}H NMR (Figure 3) indicates a similar diastereomeric ratio, i.e. 2:1 in favor of **1a**, as does a trace of the UV detector output from the preparative flash chromatography system used to separate **1a** and **1b** (Figure S19). d_2-1,1,2,2-Tetrachloroethane was used as the NMR solvent in this study due its high boiling point, which enabled the VT NMR study reported below. The diastereoselectivity is reproducible. Importantly, no discernible diastereoselectivity was reported for nonperfluorinated analogues,[30] indicating that perfluorination of the pendant ring on **6** is responsible for the diastereoselectivity encountered during the synthesis of **1a** and **1b**. We propose that this is due to more favorable intramolecular $\pi-\pi$ interactions in **1a** than in **1b** (see X-ray diffraction and VT NMR data below), as perfluorination is known to enhance $\pi-\pi$ stacking[38−41] and Ar−H and Ar−F groups exert very similar steric effects.[47] Such a combination of diastereoselectivity and clean diastereomer separation is noteworthy. The separation of diastereomeric monoiridium complexes is often challenging[48] and has previously required HPLC separation.[49] Previously reported separations have often focused on statistical distributions of isomers for which no diastereoselectivity was observed.[30,50] The only completely diastereoselective synthesis of a diastereomeric monoiridium complex that we are aware of affords complexes with poor photophysical performance due to their proline auxiliary ligands (PLQY < 10%).[32]

The complexes show good thermal stability with decomposition temperatures (T_d corresponding to 5% weight loss) of ca. 320 °C by thermal gravimetric analysis (TGA) (Figures S25 and S26).

Table 1. Selected Geometrical Parameters (Bond Distances in Å)

	1a[a]	1b
space group	$P2_1/n$	$I4_1/a$
stereochemistry	Δ_R/Λ_S	Δ_S/Λ_R
Bonds to Cyclometalating Ligands		
Ir−C (*trans*-O)	1.99(1)/2.00(1)	1.994(3)
Ir−C (*trans*-N)	2.01(1)/2.00(1)	1.999(3)
Ir−N, stacked	2.026(9)/2.02(1)	2.028(2)
Ir−N, nonstacked	2.06(1)/2.04(1)	2.049(2)
Bonds to Auxiliary Ligand		
Ir−O	2.117(8)/2.134(7)	2.137(2)
Ir−N	2.140(8)/2.14(1)	2.165(2)
deviation of phenoxy plane from Ir−N1−O1 coordination plane, deg	25.0/24.2	33.8
Intramolecular Stacking ($\pi-\pi$)		
θ, deg[b]	5.0/6.7	7.8
D, Å[c]	3.30	3.33

[a]Contains two crystallographically nonequivalent molecules. [b]Interplanar angle between pendant pentafluorophenyl ring A of the ancillary ligand and ring B of the cyclometalating ligand (pyridine for **1a**, phenyl for **1b**; see Figure 4). [c]Distance between the plane of ring B and the centroid of ring A.

Intramolecular $\pi-\pi$ Interactions. *X-ray Crystallography.* The molecular structures of **1a** and **1b** were studied by single-crystal X-ray diffraction. Important parameters are summarized in Table 1, and the structures are shown in Figure 4.

The crystals are racemic for both diastereomers, while the crystal of **1a** contains two crystallographically nonequivalent molecules (Figure S29). Complexes **1a** and **1b** both have distorted-octahedral coordination about their Ir centers as expected, with the N atoms of the cyclometalating ligands occupying positions axial to the plane of the phenoxyoxazoline

DOI: 10.1021/acs.inorgchem.8b02034
Inorg. Chem. XXXX, XXX, XXX−XXX

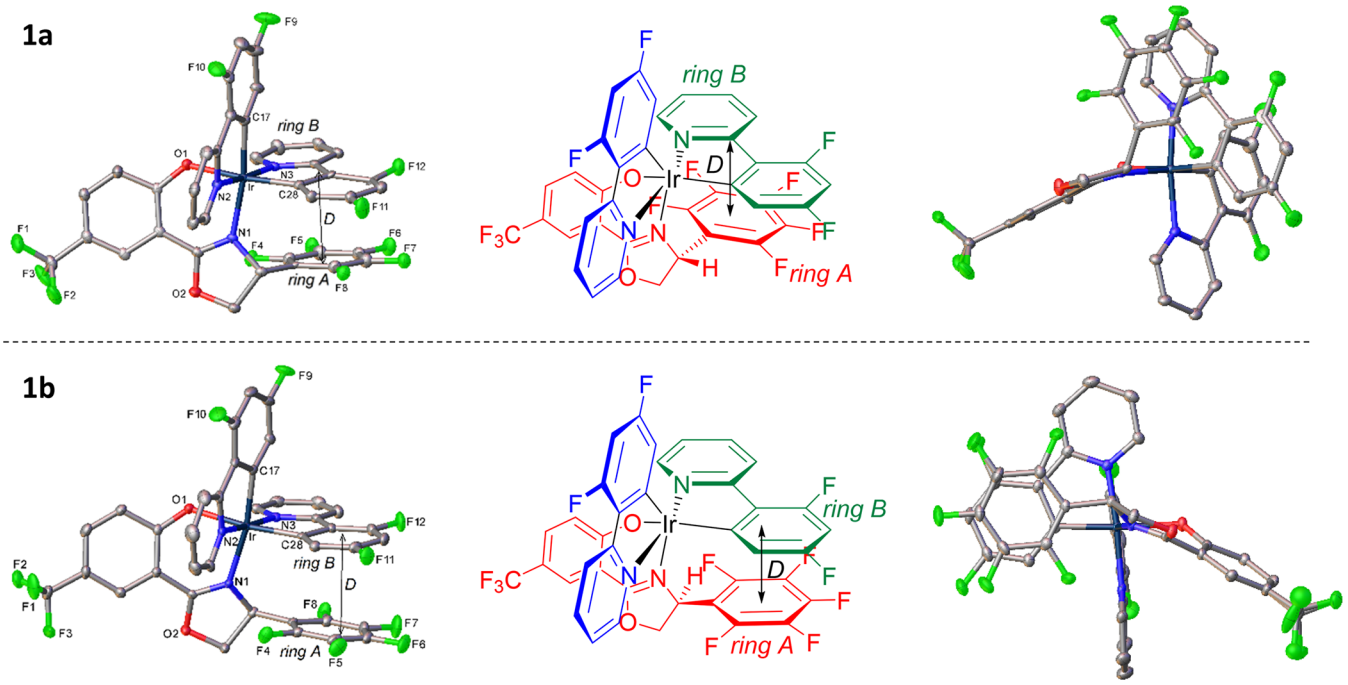

Figure 4. (top) Two depictions of the X-ray crystal structure of Δ_R-**1a**. The left OLEX2[51] perspective plot highlights intramolecular $\pi-\pi$ interactions. The central structure is drawn in the same projection as this plot to clarify the differing stereochemistry of the diastereomers. The right perspective plot is projected along the auxiliary ligand Ir−N−O coordination plane. Cyclometalating ligands are drawn in green and blue, while the auxiliary ligand is drawn in red. (bottom) Similar diagrams for Δ_S-**1b**. Thermal ellipsoids are drawn at the 50% probability level, and H atoms are omitted for clarity. Vector *D* identifies intramolecular $\pi-\pi$ interactions (see Table 1 and discussion in the text).

ligand coordination and trans to each other. The phenoxyoxazoline ligand **6** coordinates via a six-membered N^O chelate as expected.[28]

The structure of the Δ_R/Λ_S diastereomer **1a** features slipped face-to-face intramolecular $\pi-\pi$ interactions (vector *D* in Figure 4) between the pendant pentafluorophenyl group (ring A) and the pyridyl component of a cyclometalating ligand (ring B) (Figure 1). This is analogous to the case for Δ_R/Λ_S nonfluorinated analogues,[30] although the stacking in **1a** is closer (D = 3.30 Å vs 3.57 Å) due to perfluorination of the pendant aryl group, as intended.

Close intramolecular stacking (D = 3.33 Å) is also observed for the diastereomer **1b** (Figure 4, bottom). However, unlike the case for **1a**, the stacking is between the pendant pentafluorophenyl group (ring A) and one of the cyclometalating phenyl moieties (ring B). The face-to-face overlap is greater (less slipped) for **1b** than for **1a**. However, the stacking in **1b** is not as close and is less parallel (**1a**, θ = 5.0/6.7°, D = 3.30 Å; **1b**, θ = 7.8°, D = 3.33 Å; see Table 1). The stacking in both **1a** and **1b** is facilitated by distortion of the auxiliary ligand from its coordination plane to increase the intramolecular $\pi-\pi$ overlap. For **1a**, the plane of the phenoxy ring is bent from the auxiliary ligand's Ir−N−O coordination plane by 24.2/25.0°, whereas for **1b** a larger distortion of 33.8° is required to facilitate stacking. These distortions are much greater than those for literature analogues that do not feature perfluoroaryl rings (5.8−15.6°).[29,30] Such notable distortions to enhance stacking in **1a** and **1b** (particularly **1b**) highlight the effectiveness of perfluorination for promoting $\pi-\pi$ interactions.

To summarize, the intramolecular $\pi-\pi$ stacking appears to be marginally weaker in **1b** than for **1a** while also requiring a greater structural distortion of the ancillary ligand to facilitate it. This indicates that the intramolecular $\pi-\pi$ interactions are more favorable in **1a**, which is reinforced by the diastereoselectivity of the complex formation and the VT NMR data below.

Variable-Temperature ^{19}F NMR Spectroscopy. The intramolecular $\pi-\pi$ interactions in **1a** and **1b** were also studied in solution by VT ^{19}F NMR spectroscopy (Figure 5) to compliment the single-crystal X-ray data.

At 25 °C (Figure 5, top left) both diastereomers exhibit five ^{19}F environments between ca. −140 and −160 ppm of equal integration, which are assigned to the pentafluorophenyl groups. The presence of five distinct environments (in contrast to the case for the free ligand **6**, for which there are three environments; Figure S15) is ascribed to a breakdown in molecular symmetry and indicates that the intramolecular $\pi-\pi$ interactions in both **1a** and **1b** are strong enough to restrict rotation of the pendant pentafluorophenyl units in solution.[38] No such restriction of rotation is observed in the ^{1}H NMR spectra of the nonperfluorinated analogues reported by Monari, Bandini, and Ceroni, indicating that the intramolecular $\pi-\pi$ interactions in our perfluorinated derivatives are stronger.[30]

Meta ^{19}F−^{19}F coupling appears to be absent from the spectra, as previously reported for other heavily fluorinated aromatics.[38,52−56] Consequently, diastereomers **1a** and **1b** both display well-resolved triplets corresponding to the pentafluorophenyl 4-positions at room temperature. However, whereas the signals corresponding to the 2-, 3-, 4-, and 5-positions are sharp for **1a**, they are broader and less well-defined for **1b**. This suggests that rotation of the pentafluorophenyl group at room temperature is more restricted (i.e., exchange is slower) for **1a**, and this was further investigated using VT ^{19}F NMR spectroscopy.

DOI: 10.1021/acs.inorgchem.8b02034
Inorg. Chem. XXXX, XXX, XXX−XXX

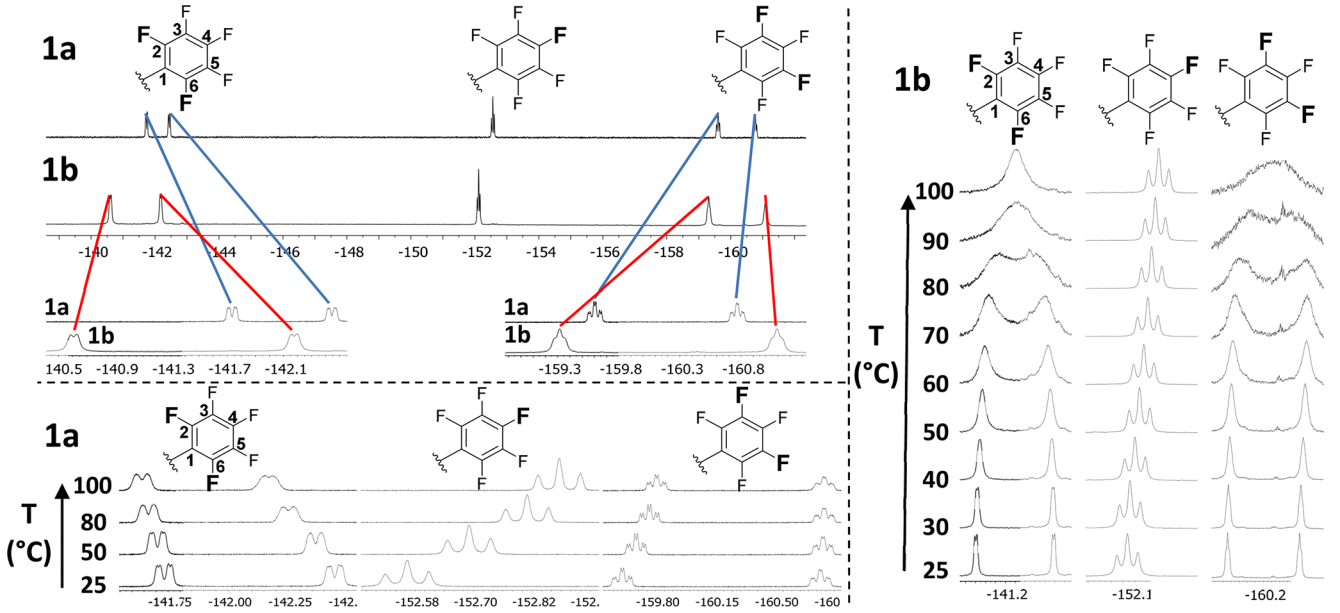

Figure 5. (top left) Expansions of the pentafluorophenyl regions of the ^{19}F NMR spectra of **1a** and **1b** at room temperature. (bottom left) VT ^{19}F NMR spectra for **1a** recorded between 25 and 100 °C. (right) VT ^{19}F NMR spectra for **1b** recorded between 25 and 100 °C. All spectra were recorded in d_2-1,1,2,2-tetrachloroethane, temperatures are ±5 °C, and chemical shifts are in ppm.

Upon heating, no significant change is observed in the shape of the triplets corresponding to the 4-positions across the entire temperature range for both **1a** and **1b**. This is expected, as the 4-positions are para to the freely rotating C−C bond.

For **1a** the signals corresponding to the 2- and 6-positions slightly broaden upon heating to 100 °C, resolving into doublets (Figure 5, bottom left). They also move toward one another, although at 100 °C they are still far from their coalescence point—their frequency difference ($\delta\nu$) is ca. 330 Hz at 25 °C, which decreases to ca. 250 Hz at 100 °C. Similarly, the signals corresponding to the 3- and 5-positions slightly broaden upon heating, while $\delta\nu$ decreases from ca. 550 Hz at 25 °C to ca. 460 Hz at 100 °C. These changes indicate that the rate at which the pendant pentafluorophenyl ring rotates increases with temperature. However, as none of the signals are close to coalescing at 100 °C, it is concluded that exchange is slow across the entire studied temperature range and that a significant energetic barrier exists for rotation of the pendant pentafluorophenyl ring of **1a**.

The VT NMR data for **1b** (Figure 5, right) contrast with those obtained for **1a**, as the rate of exchange for **1b** increases more drastically with temperature. The signals corresponding to the 2- and 6-positions ($\delta\nu$ at 25 °C ca. 740 Hz) and the 3- and 5-positions ($\delta\nu$ at 25 °C ca. 835 Hz) coalesce at ca. 85 °C and ca. 95 °C, respectively. This is because upon heating the pentafluorophenyl ring of **1b** starts to rotate sufficiently quickly that the 2- and 6-positions become indistinguishable on the NMR time scale (millisecond scale in this case—see discussion in the Supporting Information). The same applies to the 3- and 5-positions. As coalescence is observed for **1b**, the free energy barrier to exchange ($\Delta G^{\ddagger}$) can be tentatively estimated at 70 kJ mol^{-1} (see the Supporting Information).[57] This value is comparable to the room-temperature $\Delta G^{\ddagger}$ value of ca. 80 kJ mol^{-1} reported by Cozzi and Siegel et al. for rotation of intramolecularly stacked perfluoroaryl rings in diarylnaphthalenes.[40,41]

Importantly, coalescence is observed for **1b**, but not **1a**. From this it is clear that intramolecular $\pi-\pi$ interactions are more effective at restricting rotation of the pentafluorophenyl ring in **1a**. This is in agreement with the more favorable stacking observed in **1a** by X-ray diffraction above.

Electrochemical and Photophysical Properties. The oxidation and reduction potentials for **1a** and **1b** were obtained via cyclic voltammetry (CV). The key data are given in Table 2, and the voltammograms are shown in Figure S20.

Table 2. Electrochemical Data for Complexes 1a and 1b Referenced to $E_{1/2}$(FcH/FcH$^+$) = 0.00 V

complex	E^{ox}/V, E_{pa}/E_{pc} [$E_{1/2}$/V]	E^{red}_{onset}/V[a]	HOMO/eV[b]	LUMO/eV[c]	E_g/V[d]
1a	0.88, 0.69 [0.78]	−2.37	−5.58	−2.43	3.15
1b	0.87, 0.74 [0.81]	−2.35	−5.61	−2.45	3.16

[a]All reductions are electrochemically irreversible. [b]HOMO levels calculated from CV potentials by HOMO = −4.8 + ($-E_{1/2}^{ox}$), using ferrocene as the standard. [c]LUMO levels calculated from CV potentials by LUMO = −4.8 + ($-E^{red}_{onset}$), using ferrocene as the standard. [d]Estimated electrochemical HOMO−LUMO gap.

Diastereomers **1a** and **1b** both display electrochemically reversible oxidations. The variation between their oxidation potentials is minimal (30 mV), as expected for diastereomers.[38,58,59] The oxidations were determined to be chemically reversible over 10 cycles for both **1a** and **1b** (Figure S21).

The estimated reduction potentials for **1a** and **1b** are typical for ppy-based cyclometalated heteroleptic Ir complexes (i.e., within ca. 2.2−2.8 V).[60] While their irreversibility adds error to their accurate determination, it is clear from the voltammograms that the reduction potentials of **1a** and **1b** are similar (within 20 mV), as expected. Because of their similar redox potentials, the electrochemical band gaps (E_g) for **1a** and **1b** are practically identical.

The absorption and emission spectra for **1a** and **1b** are shown in Figure 6, and the key data are given in Table 3. The

DOI: 10.1021/acs.inorgchem.8b02034
Inorg. Chem. XXXX, XXX, XXX−XXX

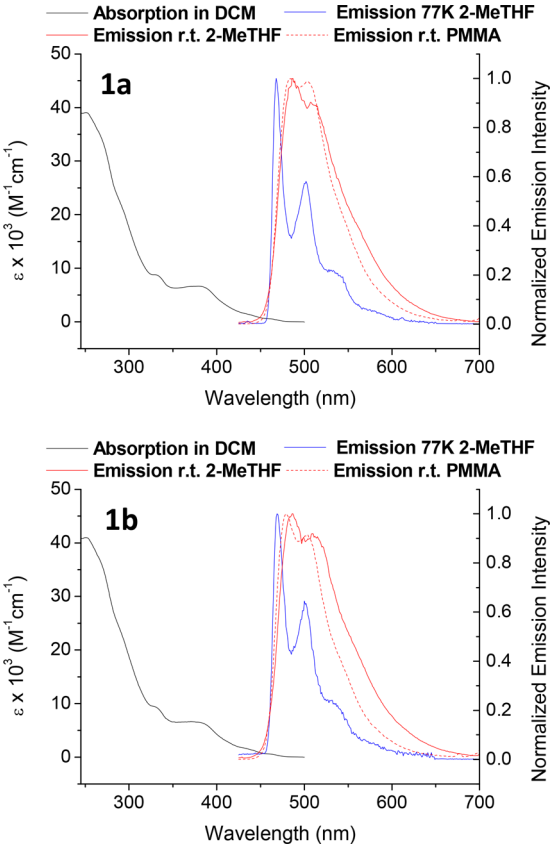

Figure 6. Absorption and PL spectra of **1a** and **1b**; λ_{ex} = 355 nm.

absorption spectra for both diastereomers are very similar and display profiles and extinction coefficients typical of cyclometalated Ir complexes.[60,61] The bands below 300 nm are ascribed to spin-allowed ligand-centered (LC) $^1\pi-\pi^*$ transitions, while the longer wavelength bands which extend to 490 nm are assigned to both singlet and triplet metal to ligand charge transfer states (^{1}MLCT and ^{3}MLCT).[61]

The PL properties of **1a** and **1b** in degassed 2-MeTHF solution at 20 °C are identical within experimental error. They each display broad profiles with subtle vibronic features, indicative of emission from admixed ^{3}LC/^{3}MLCT states,[62] with full-width half-maxima (fwhm) of ca. 80 nm. The PLQYs of **1a** and **1b** are ca. 50%, and their phosphorescence lifetimes are around 1.5 μs. These data are within the range reported for Ir(III) complexes with 2-phenoxyazole auxiliary ligands, including nonperfluorinated analogues of **1a** and **1b**, and are typical of heteroleptic phosphorescent iridium complexes.[16,26,60] **1a** and **1b** display the same 77 K emission spectra in 2-MeTHF, with estimated Huang–Rhys factors and triplet energies (E_T) of 0.6 (1 s.f.) and 2.70 eV, respectively. This similarity in the photophysical properties between **1a** and **1b** is important information for future work, demonstrating that diastereomeric mixtures of monoiridium complexes can be studied without concern that the diastereomers are behaving differently.

When they are doped into poly(methyl methacrylate) (PMMA), both **1a** and **1b** feature longer τ values of ca. 1.7 μs. The PLQYs are slightly increased to 60/67 ± 10%, although within experimental error they are similar to the solution values. This can mainly be attributed to decreases in k_{nr}, due to the more rigid PMMA matrix, although there is also a small increase in the radiative rate constant (k_r) for both complexes. Despite very similar lifetimes and PLQYs in PMMA, a noteworthy difference is observed between the spectral profiles of **1a** and **1b**. Doping either complex into PMMA leads to PL spectra that are blue-shifted (by 2 nm for **1a** and 8 nm for **1b**) and narrower (fwhm: **1a**, ca. 70 nm; **1b**, 65 nm) than in 2-MeTHF solution. These effects are more pronounced for **1b** and may be related to either the higher rigidity of PMMA in comparison to 2-MeTHF or its polarity.

While **1a** and **1b** display similar PL properties at room temperature and 77 K, the VT NMR data above suggest that they may display different photophysical properties at elevated temperatures, prompting a high-temperature PL study. The PL spectra of **1a** and **1b** in xylenes upon cycling the temperature between 30 and 100 °C are shown in Figure 7.

Upon heating from 30 to 100 °C the emission intensities for both complexes decrease. The decrease in intensity is not due to decomposition or ingress of oxygen, as the initial spectral intensities are retained upon cooling back to 30 °C. The normalized spectral profiles do not change for either diastereomer (shown for **1b** in Figure S22), suggesting that PL originates from the same state at both temperatures. A decrease in the emission intensities of **1a** and **1b** upon heating implies the existence of a temperature-dependent

Table 3. Photophysical Properties of Complexes 1a and 1b

		2-MeTHF soln[b]				
complex	DCM soln λ_{abs}/nm (ε/10^3 M^{-1} cm^{-1})	$\lambda_{max,em}$/nm [CIE$_{xy}$]	PLQY/% (±5%)	τ/μs	k_r/10^5 s^{-1}	k_{nr}/10^5 s^{-1}
1a	251 (39), 270 sh[a] (33), 291 sh (22), 332 (8.7), 383 (6.5), 439 sh (1.3), 464 (0.5), 490 (0.1)	487 [0.23, 0.49]	51	1.56	3.27	3.14
1b	252 (41), 269 sh (36), 290 sh (23), 332 (9.0), 384 (6.3), 438 sh (1.4), 465 (0.5), 490 (0.1)	487 [0.24, 0.49]	50	1.54	3.25	3.25

	2-MeTHF glass[c]			doped into PMMA 1 wt %[d]			
complex	$\lambda_{max,em}$/nm ($\lambda_{10\%,em}$ /nm)[e] [E_T/eV][f]	τ/μs	$\lambda_{max,em}$/nm [CIE$_{xy}$]	PLQY/% (±10%)	τ/μs	k_r/10^5 s^{-1}	k_{nr}/10^5 s^{-1}
1a	468 (459) [2.70]	2.79	485 [0.18, 0.46]	67	1.72	3.90	1.92
1b	469 (459) [2.70]	2.49	479 [0.17, 0.42]	60	1.73	3.47	2.31

[a]sh = shoulder. [b]Solution photoluminescence measurements were recorded in degassed 2-MeTHF solutions at ca. 20 °C with an excitation wavelength of 355 nm with quinine sulfate in 0.5 M H_2SO_4 as standard (Φ = 0.546);[16] under the same experimental conditions a value of 73 ± 5% was obtained for FIrpic. [c]Measured at 77 K using an excitation wavelength of 355 nm. [d]Measured in an integrating sphere in air using an excitation wavelength of 355 nm. [e]Wavelength at 10% intensity on the blue edge of the spectrum obtained at 77 K. [f]Estimated using $E_T = hc/\lambda_{10\%,em}$. $\tau = 1/k_{nr} + k_r$.

DOI: 10.1021/acs.inorgchem.8b02034
Inorg. Chem. XXXX, XXX, XXX–XXX

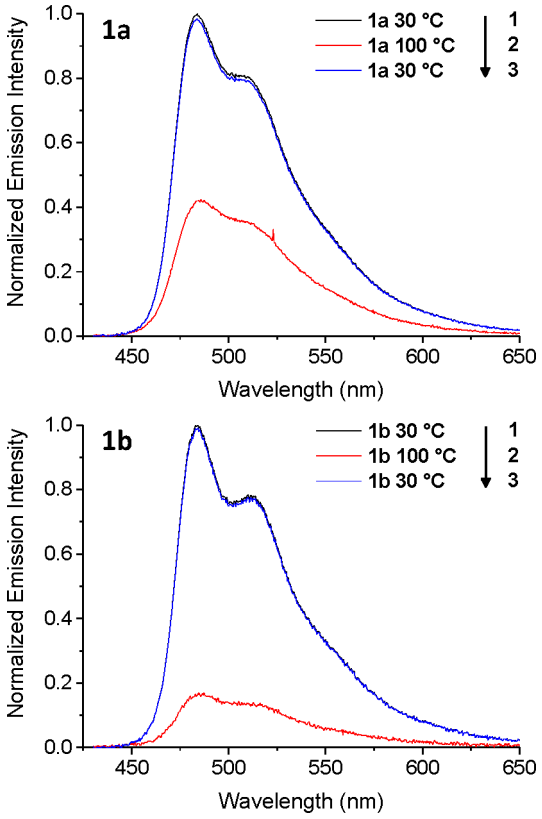

Figure 7. Variable-temperature PL spectra of **1a** and **1b** recorded in degassed xylenes. The spectra are normalized to the initial emission intensity at 30 °C. Temperatures are ±5 °C and λ_{ex} is 405 nm. The numbers refer to the order in which the spectra were run.

nonradiative pathway which becomes more accessible at higher temperatures. For cyclometalated iridium complexes this has been ascribed to the thermal population of low-lying metal-centered (MC) states.[62,63]

The integrated emission intensity for **1a** drops to 44% of its initial intensity upon heating to 100 °C, whereas it drops to 18% for **1b**. Both complexes have the same solution PL λ_{max}, PLQY, and phosphorescence lifetime, display identical E_T values, and have the same coordination environment about their Ir centers. Therefore, the energy gaps between the MC and emitting states for **1a** and **1b** are expected to be very similar, meaning that nonradiative deactivation via thermally accessible MC states alone cannot explain such a significant difference in the temperature dependence of their PL properties. The VT ^{19}F NMR data above indicate that there is a smaller energy barrier to rotation of the C_6F_5 ring in **1b**. Therefore, such rotation can be expected to constitute a more easily populated nonradiative pathway for **1b** than for **1a**, which leads to a more substantial decrease in emission intensity upon heating for **1b** and explains the observed differences in the high-temperature PL data.

Computational Study. Electronic structure calculations were carried out on **1a** and **1b** to explore their molecular orbitals and to support their electrochemical and photophysical properties. The optimized S_0 geometries were calculated at the B3LYP/LANL2DZ:6-31G* level. They are in good agreement with the X-ray crystallographic data above—intramolecular $\pi-\pi$ interactions are observed for both diastereomers and the auxiliary ligand of **1b** is more distorted. Complex **1a** is less stable than **1b** by 2.3 kJ mol^{-1}, suggesting that **1a** is the kinetic product, although it could not be isomerized to **1b** photochemically.

Molecular orbital plots for the highest occupied molecular orbitals (HOMO) and lowest unoccupied molecular orbitals (LUMO) of **1a** and **1b** are shown in Figure 8. Further plots and tabulated contributions for the HOMO-1−LUMO+2 orbitals are given in Figure S23 and Table S1.

The HOMO−1−LUMO+2 compositions are nearly identical for both complexes. The HOMOs are primarily localized on the phenoxy moieties of the auxiliary ligands (55%) and the Ir atoms (25%), with small contributions from the cyclometalating phenyl groups (ca. 10%). This suggests that the CF_3 and oxazoline-functionalized phenoxy moiety is more electron rich than a cyclometalated dfppy ring. The LUMOs are almost exclusively localized on the cyclometallating ligands with ca. 70% and 25% contributions from the pyridyl and phenyl moieties, respectively. Therefore, the FMO contributions for **1a** and **1b** are in good agreement with previous complexes that feature a phenoxyoxazole auxiliary ligand.[29] It should be noted that there is no LUMO contribution from the pendant pentafluorophenyl groups for either **1a** or **1b**.

Time-dependent density functional theory (TD-DFT) was also employed to simulate the absorption spectra of **1a** and **1b** and to investigate the character of their lowest energy excited states (Figure S24 and Table S2). The simulated absorption spectra for both complexes broadly agree with the experimental data, while the predicted lowest energy triplet states of both **1a** and **1b** are mainly localized, as expected from analysis of their frontier molecular orbitals (HOMO and

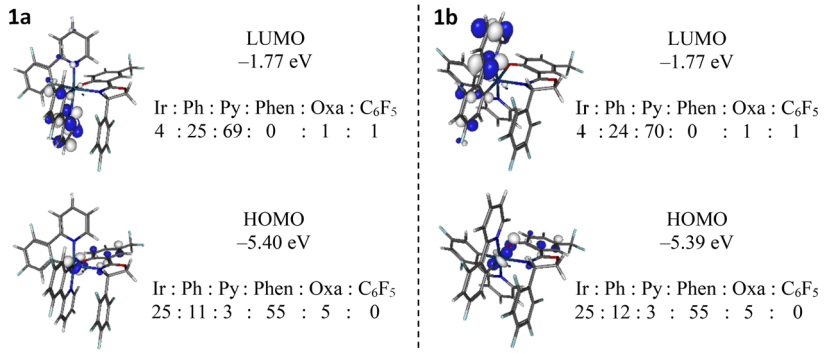

Figure 8. Molecular orbital compositions for **1a** and **1b**. Contributions are percentages. Abbreviations: Ph = phenyl, Py = pyridyl, Phen = phenoxy, Oxa = oxazoline.

DOI: 10.1021/acs.inorgchem.8b02034
Inorg. Chem. XXXX, XXX, XXX−XXX

LUMO) (a more detailed discussion is included in the Supporting Information). Both DFT and TD-DFT data suggest that any contributions from the pentafluorophenyl groups to the excited states of **1a** and **1b** are small, rendering them ancillary.

PhOLEDs. To evaluate the major diastereomer **1a** as an emitter in PhOLEDs, devices were fabricated in the following configuration: ITO/TAPC (30 nm)/mCP (10 nm)/PPF: **1a** (30 nm)/B_3pympm (30 nm)/LiF/Al. The devices were fabricated by thermal evaporation onto a cleaned glass substrate precoated with conductive transparent indium tin oxide (ITO), where 4,4′-cyclohexylidenebis[*N*,*N*-bis(4-methylphenyl)benzenamine] (TAPC) served as a hole-transporting layer, 1,3-bis(carbazol-9-yl)benzene (mCP) as an electron/exciton-blocking layer (EBL) between TAPC and the emissive layer, 4,6-bis(3,5-bis(pyridin-3-yl)phenyl)-2-methylpyrimidine (B_3pympm) as an electron-transporting layer, and 2,8-bis(diphenylphosphoryl)dibenzofuran (PPF) as the host. Devices were fabricated with doping levels of **1a** of 3.5, 8, and 15 wt %. The device data are summarized in Table 4. Data are plotted for the best-performing device (8 wt %) in Figure 9; comparable data for the 3.5 and 15 wt % devices are presented in Figures S27 and S28. Generally, the most commonly used and suitable concentration of an Ir complex for doping PhOLEDs is 5−10 wt %.[6−12] Indeed, our results in this manuscript confirmed this, as the devices employing 8 wt % showed the highest performance. Here, other devices adopting lower (3.5 wt %) and higher (15 wt %) concentrations of **1a** were also fabricated to investigate the dependence of the doping concentration on the EL performance, as discussed below.

Table 4. Device Data for 1a

wt %	V_{on}/V[a]	L_{max}/cd m^{-2} [b]	EQE/%[c]	PE/lm W^{-1} [c]	CIE$_{xy}$ [d]
3.5	4.7	9190	23.6, 23.5, 19.1	34.0, 28.5, 15.3	0.17, 0.46
8	4.3	31480	25.8, 25.3, 24.9	42.3, 33.6, 24.8	0.17, 0.48
15	4.0	21870	24.3, 23.7, 23.1	41.9, 31.2, 22.0	0.18, 0.50

[a]Applied voltage required to reach a luminance of 1 cd m^{-2}. [b]L_{max} = maximum luminance. [c]The efficiencies listed are the maximum values and the values at 100 and 1000 cd m^{-2}, respectively. [d]Recorded at 1000 cd m^{-2}.

The electroluminescence (EL) spectrum of the 8 wt % device at 100 cd m^{-2} is consistent with the PL spectrum recorded for **1a** in PMMA, although the EL spectrum is narrower (by 15 nm). The device displays a turn-on voltage of 4.3 V. It also features a high maximum external quantum efficiency (EQE$_{max}$) of 25.8% (at ca. 270 cd m^{-2}) with a low efficiency roll-off to 24.9% at 1000 cd m^{-2}, which is better than previously reported data for other heteroleptic complexes functionalized with phenoxyoxazole/thiazole auxiliary ligands.[28,29] However, the maximum brightness and luminance efficiency are lower in comparison to the previous derivatives. The overall EL performance for the 3.5 wt % device is poorer than that for the 8 wt % devices (Table 4). This is presumably because of the low content of the dopant molecules, which means that almost all holes and/or electrons must inject into the emissive layer from the host molecules. For this to occur, the large energy barriers between the charge transport layers and emissive layer due to the rather wide HOMO−LUMO gap of the host must be overcome, resulting in a high buildup of charge carriers at the corresponding interfaces. The decreased performance of the 15 wt % device is likely due to an increased probability of triplet−triplet annihilation.

Notably, the maximum EQE, power efficiency (PE), and luminance efficiency (L_{max}) values for 8 wt % **1a** are either notably better than or highly competitive with those obtained by Shan, Xie, Su, et al. for a device doped with a different pentafluorophenyl-functionalized heteroleptic Ir complex (maximum EQE = 10.7%, maximum PE = 27.6 lm W^{-1}, L_{max} = 32710 cd m^{-2}).[64] At 10000 cd m^{-2} an EQE of >15% is maintained for the device doped with 8 wt % **1a**, in comparison with ca. 10% reported by Shan, Xie, Su, et al. at this brightness. These new data provide a further example for which multifluorination of an Ir(III) phosphor does not mandate poor PhOLED performance. This is in contrast to what would be expected considering that only four aromatic fluorine atoms are known to adversely effect the PhOLED performance of FIrpic, and **1a** incorporates an additional five Ar−F groups (nine in total).[65−67] This is likely related to the ancillary nature of the additional aromatic fluorine atoms on the pentafluorophenyl substituent in **1a**, which is also the case for the example presented by Shan, Xie, Su ,and co-workers.[64] Literature precedent from work on emitters for light-emitting electrochemical cells suggests that the intramolecular $\pi-\pi$ interactions in **1a** may also play a significant role in the good device performance.[33]

Conclusions. In conclusion, the new diastereomeric Ir complexes **1a** and **1b** were obtained in a 2:1 ratio. They were easily separated, and their structural, electrochemical, and photophysical properties were studied in detail.

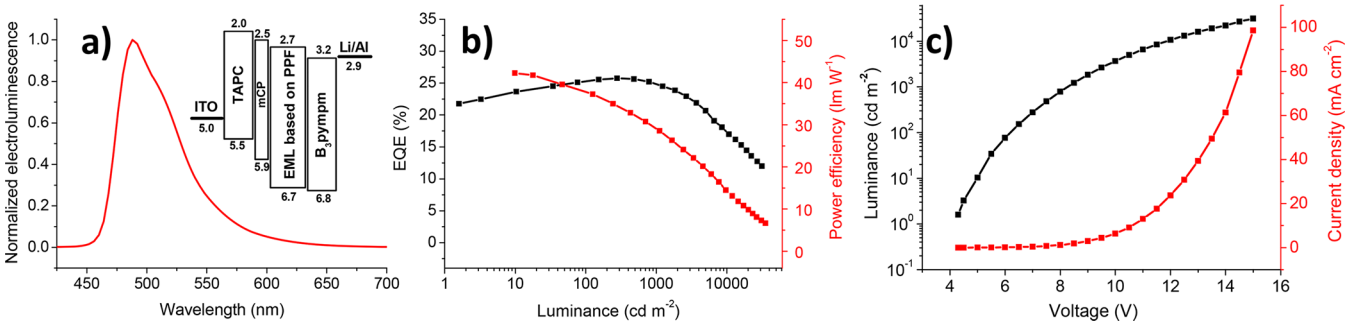

Figure 9. PhOLED data (8 wt %) for **1a**: (a) EL spectrum at a luminance of 100 cd m^{-2} (inset: energy level diagram for the device (eV)); (b) external quantum efficiency and power efficiency curves vs voltage; (c) luminance and current density curves vs voltage.

DOI: 10.1021/acs.inorgchem.8b02034
Inorg. Chem. XXXX, XXX, XXX−XXX

In both diastereomers the pendant pentafluorophenyl ring on the chiral auxiliary ligand engages in close (D = ca. 3.3 Å) intramolecular $\pi-\pi$ stacking with a cyclometalating ligand on the periphery of the complexes. The intramolecular $\pi-\pi$ stacking was studied in the solid state by single-crystal X-ray diffraction and in solution by VT ^{19}F NMR. The interactions are stronger in **1a**, leading to the observed diastereoselectivity. The different intramolecular $\pi-\pi$ interactions in **1a** and **1b** have little influence on their photophysical properties at room temperature. This is likely because the interactions occur on the periphery of an already highly emissive Ir complex core. However, upon heating to high temperatures the weaker intramolecular $\pi-\pi$ interactions in **1b** provide a more efficient thermally activated pathway to quench phosphorescence through rotation of the pentafluorophenyl ring. Overall the photophysical differences between **1a** and **1b** are small. Nevertheless, the separation and study of diastereomeric Ir(III) phosphors in detail is still relatively rare and further enhances the understanding of the effects of stereochemistry on the photophysical properties of Ir(III) complexes.

This study also enriches the literature on phosphorescent Ir complexes, especially related to the effects of intramolecular $\pi-\pi$ interactions and ancillary aromatic fluorine atoms on structural and photophysical properties. This is evident from PhOLED results: a vacuum-processed PhOLED doped with **1a** as the emissive dopant gave a high EQE_{max} and low efficiency roll-off (EQE 24.9% at 1000 cd m^{-2}) for a complex with such a highly fluorinated aryl substituent. This is likely related to the ancillary nature of the pentafluorophenyl group, which is predicted by DFT/TD-DFT for both **1a** and **1b**. Future work should address the significance of ancillary fluorine atoms on the stability of Ir complexes, as this may provide new insights into designing highly fluorinated Ir(III) complexes that improve upon complexes such as FIrpic, for which the nonancillary fluorine atoms are known to be a source of instability.[65,68]

EXPERIMENTAL SECTION

General Considerations. ^{1}H, ^{13}C, and ^{19}F NMR spectra were recorded on Bruker Avance 400 MHz, Varian Mercury 400 MHz, Varian Inova 500 MHz, and Varian VNMRS 600 MHz spectrometers. All spectra were referenced against the residual solvent signal, and peak shifts are reported in ppm. Electrospray ionization (ESI) mass spectra were recorded on a Waters Ltd. TQD spectrometer. Elemental analyses were obtained on an Exeter Analytical Inc. CE-440 elemental analyzer. Thermal analysis was run under a helium atmosphere at a rate of 10 °C min^{-1} using a PerkinElmer Pyris 1 instrument. Melting points were determined in open-ended capillaries using a Stuart Scientific SMP3 melting point apparatus at a ramp rate of 3 °C min^{-1} and are uncorrected. Reactions requiring an inert atmosphere were carried out under argon, which was first passed through a phosphorus pentoxide column. For reaction monitoring analytical thin-layer chromatography (TLC) was carried out on silica gel (Merck, silica gel 60, F254) or alumina (Merck, neutral alumina 60 type E, F254) plates and visualized using UV light (254, 315, 365 nm). GCMS data were recorded on a Thermo-Finnigan Trace GCMS instrument. Flash chromatography was carried out using either glass columns or a Biotage Isolera One automated flash chromatography machine on 60 μm silica gel purchased from Fluorochem Ltd. All commercial chemicals were of ≥95% purity and were used as received without further purification. All solvents used were of analytical reagent grade or higher. Anhydrous solvents were dried through a HPLC column on an Innovative Technology Inc. solvent purification system or obtained commercially.

Calculations. All calculations were carried out with the Gaussian 09 package.[69] All optimized S_0 geometries of the iridium complexes were carried out using B3LYP[70,71] with the pseudopotential (LANL2DZ)[72−74] for iridium and 6-31G* basis set for all other atoms.[75,76]All S_0 geometries were true minima based on no imaginary frequencies found. Electronic structure calculations were also carried out on the optimized geometries at the B3LYP/LANL2DZ:6-31G* level. The MO diagrams and orbital contributions were generated with the aid of Gabedit[77] and GaussSum[78] packages, respectively.

X-ray Crystallography. X-ray diffraction experiments were carried out on a Bruker three-circle D8 Venture diffractometer with a PHOTON 100 CMOS area detector, using Mo Kα radiation from an Incoatec IμS microsource with focusing mirrors (λ = 0.71073 Å) and a Cryostream open-flow N_2 gas cryostat. The structures were solved by direct methods (SHELXS[79]) and refined by full-matrix least squares using SHELXL[80] programs on an OLEX2 platform.[51]

Crystal data are as follows: **1a**, $C_{38}H_{18}F_{12}IrN_3O_2$, M_r = 968.75, monoclinic, space group $P2_1/n$ (No. 14), a = 11.2459(6) Å, b = 15.8876(9) Å, c = 36.256(2) Å, β = 96.748(1)°, V = 6433.0(6) Å^3, Z = 8, D_x = 2.000 g cm^{-3}, μ = 4.26 mm^{-1}, T = 120 K, 78522 data with $2\theta \leq 50.7°$ (11783 unique, R_{int} = 0.085), R_1 = 0.071 on 8751 data with $I > 2\sigma(I)$, wR_2 = 0.150 on all data, CCDC-1850087; **1b**, tetragonal, space group $I4_1/a$ (No. 88), a = 19.2978(8) Å, c = 34.5207(15) Å, V = 12855.7(12) Å^3, Z = 16, D_x = 2.002 g cm^{-3}, μ = 4.27 mm^{-1}, T = 120 K, 110471 data with $2\theta \leq 58°$ (8529 unique, R_{int} = 0.070), R_1 = 0.025 on 6701 data with $I > 2\sigma(I)$, wR_2 = 0.049 on all data, CCDC-1850088.

Electrochemistry. Cyclic voltammetry data were recorded using a BAS CV50W electrochemical analyzer fitted with a three-electrode system consisting of a glassy-carbon disk (i.d. = 1.8 mm) as the working electrode, a Pt wire as the auxiliary electrode, and a Pt wire as the quasi-reference electrode.. Experiments were conducted in dry THF solution with n-Bu_4NPF_6 (0.1 M) as the supporting electrolyte at a scan rate of 100 mV s^{-1}. All potentials were referenced internally to ferrocene.

Photophysics. The absorption spectra were measured on either a Unicam UV2-100 spectrometer operated with Unicam Vision software or a Thermo Scientific Evolution 220 spectrometer with Thermo Scientific Insight software in quartz cuvettes with a path length of 10 mm. Pure solvent (DCM) was used for the baseline correction. The extinction coefficients were calculated using the Beer−Lambert Law: $A = \varepsilon cl$. They were measured using a titration method, whereby a stock solution of known concentration was incrementally added using a calibrated glass pipet to a cuvette of pure solvent. A minimum of 1 mg of sample was weighed out for the stock solutions, and the measurements were carried out in triplicate to minimize weighing and dilution error. Photoluminescence spectra were recorded on a Horiba Jobin Yvon SPEX Fluorolog 3-22 spectrofluorometer in quartz cuvettes with a path length of 10 mm. All solutions were degassed via multiple freeze−pump−thaw cycles using a turbomolecular pump before acquisition of any spectra. For quantum yield measurements the absorption values for the samples were determined on a Unicam UV2-100 spectrometer operated with Unicam Vision software in quartz cuvettes with a path length of 20 mm. The PLQYs of all samples were determined in triplicate by a comparative method relative to a literature standard following the literature procedure.[58] PMMA films were prepared according to a literature procedure.[38] The quantum yields of complexes doped into PMMA were recorded on a Horiba Jobin Yvon SPEX Fluorolog 3 instrument using a calibrated Quanta-Φ integrating sphere and were calculated according to the literature method.[81] Solid-state PLQY data were obtained in triplicate from three samples that were prepared in parallel: the calculated standard error values were ≤10%. Lifetime measurements were recorded using an N_2 laser (337 nm, 10 μJ, 10 Hz) as an excitation source in a custom spectrometer which produced a 1 kHz train of pulses of 20 ns duration. The luminescence was collected at 90° and focused onto the entrance slit of a monochromator (Bethan TM 300 V). The emission was detected by a photon counting PMT, and the arrival times of photons at the detector were determined using a multichannel scaler. The data were

DOI: 10.1021/acs.inorgchem.8b02034
Inorg. Chem. XXXX, XXX, XXX−XXX

transferred to a PC and analyzed using nonlinear regression. The decay data were fitted to exponential functions. Low-temperature emission spectra and lifetime data were measured in a DN1704 optical cryostat (Oxford Instruments) with an ITC601 temperature controller (Oxford Instruments). For high-temperature PL measurements, samples were degassed via multiple freeze−pump−thaw cycles in an NMR tube fitted with a Young tap. The sample was heated in a silicone oil bath. A 405 nm laser was focused on the sample perpendicular to the detector of an Ocean Optics Maya Pro spectrometer.

PhOLED Fabrication and Measurements. Prior to the fabrication of the devices, patterned indium tin oxide (ITO) coated glass substrates (20 Ω/square) were first cleaned in detergent solutions, followed by deionized water, acetone, and isopropyl alcohol ultrasonic baths. Then, the ITO substrates were treated using a Plasma Cleaner (PDC-32G-2, 100 W) with the oxygen ambient for 5 min to increase the work function. The OLEDs were fabricated by thermal evaporation at a pressure of ca. 3.5×10^{-4} Pa. All organic materials were purified by sublimation and were continuously deposited onto the substrate at the rate of 0.3 Å s^{-1}, and then a very thin layer of LiF (0.5 nm) was deposited at a rate of 0.2 Å s^{-1} and the Al electrode (cathode) was deposited at a rate of 3.0−4.0 Å s^{-1}, where the active area of the diode segments was 2×2.5 mm^2. The EL spectra and CIE coordinates of the devices were measured using a PR650 spectrometer. The current density−voltage−luminance curves of the devices were measured using a Keithley 2400 source meter. EQEs were calculated from the *J*−*V*−*L* characteristics and EL spectra. All characterizations were carried out under ambient conditions at room temperature.

Synthesis. Compounds **3** and **4**[46] and $[Ir(dfppy)_2(\mu\text{-}Cl)]_2$[82] were synthesized according to literature procedures.

*rac-4-(Pentafluorophenyl)-2-(2-hydroxy-5-trifluoromethylphenyl)-oxazoline (**6**).*

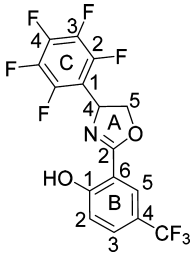

rac-2-Amino-2-(pentafluorophenyl)ethanol (**4**; 1.21 g, 5.33 mmol, 1.21 equiv) and 2-hydroxy-5-trifluoromethylbenzonitrile (**5**; 829 mg, 4.40 mmol, 1.00 equiv) were combined in dry toluene (12 mL). A solution of $ZnCl_2$ in THF was added (0.7 M, 0.31 mL, 0.22 mmol, 5 mol %), and the resulting mixture was heated to reflux for 20 h. The reaction mixture was cooled to room temperature and evaporated under reduced pressure. The residue was purified by flash chromatography on silica gel (eluent: gradient 1/0 to 1/3 *n*-hexane/DCM with ca. 0.5% NEt_3 as additive) to afford *rac*-4-(pentafluorophenyl)-2-(2-hydroxy-5-trifluoromethylphenyl)oxazoline (**7**) as a white powder (730 mg, 1.80 mmol, 41%): mp 117−119 °C; ^{1}H NMR (700 MHz, $CDCl_3$) δ (ppm) 11.91 (s, $1H_{OH}$), 8.02 (d, J = 2.3 Hz, $1H_{B5}$), 7.64 (dd, J = 8.8, 2.3 Hz, $1H_{B3}$), 7.09 (d, J = 8.8 Hz, $1H_{B2}$), 5.83 (dd, J = 10.7, 7.6 Hz, $1H_{A4}$), 4.81 (dd, J = 10.7, 8.8 Hz, $1H_{A5}$), 4.51 (dd, J = 8.2, 7.6 Hz, $1H_{A5}$); ^{13}C NMR (101 MHz, $CDCl_3$) δ (ppm) 166.5 (C_{A2}), 161.3 (C_{B1}), 146.0−136.0 ($C_{ring\ C}$), 130.7 (C_{B3}), 126.2 (C_{B5}), 123.9 (q, J = 270 Hz, C_{CF3}), 121.4 (q, J = 32.3 Hz, C_{B4}), 117.6 (C_{B2}), 109.9 (C_{B6}), 71.2 (C_{A5}), 58.93 (C_{A4}); ^{19}F{^{1}H} NMR (376 MHz, $CDCl_3$) δ (ppm) −61.7 (d, J = 1.1 Hz, $3F_{CF3}$), −143.3 to −143.5 (m, $2F_{C2}$), −153.1 (ddt, J = 23.1, 21.0, 2.2 Hz, $1F_{C4}$), −160.9 to −161.1 (m, $2F_{C3}$); HRMS (ESI) m/z 398.0459 [MH^+], calcd for $C_{16}H_8F_8NO_2^+$ 398.0422. Due to extensive coupling to ^{19}F nuclei, the ^{13}C signals for ring C are stated as a range.

*Complexes **1a** and **1b**.* $[Ir(dfppy)_2(\mu\text{-}Cl)]_2$ (315 mg, 0.26 mmol, 1.00 equiv), *rac*-4-(pentafluorophenyl)-2-(2-hydroxy-5-trifluoromethylphenyl)oxazoline (**6**; 211 mg, 0.53 mmol, 2.05 equiv), and K_2CO_3 (90 mg, 0.65 mmol, 2.50 equiv) were combined in dry diglyme (10 mL) under argon and heated in a 140 °C heating mantle overnight under argon. The reaction mixture was cooled to room temperature and the solvent evaporated under reduced pressure. Repeated coevaporation with toluene to remove the final traces of diglyme was beneficial to obtain facile separation of **1a** and **1b**. The residue was purified by flash chromatography on silica gel (eluent: gradient 1/9 to 4/6 DCM saturated K_2CO_3/*n*-hexane v/v) to elute **1a**. Increasing the solvent polarity to 6/4 DCM saturated K_2CO_3/*n*-hexane v/v eluted **1b**. Each diastereomer was further purified through dissolving it in minimal DCM (ca. 10 mL), adding *n*-hexane (30 mL) and reducing the solvent volume to ca. 15 mL to induce precipitation. After the mixture was cooled in a freezer for ca. 1 h, the precipitates were isolated via filtration and washed with ice-cold pentane before being dried under high vacuum.

*Complex **1a**.*

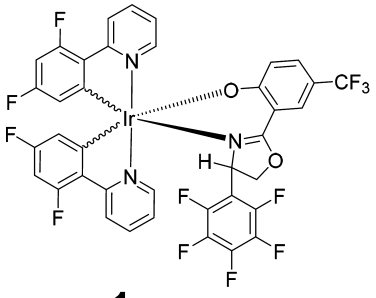

1a

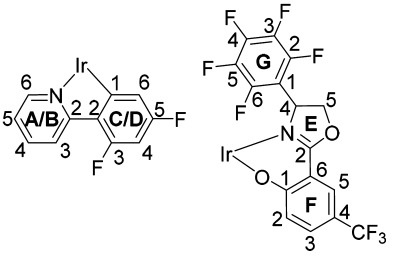

Isolated as a yellow microcrystalline powder (331 mg, 0.34 mmol, 66%): ^{1}H NMR (600 MHz, d_2-1,1,2,2-TCE) δ (ppm) 8.76 (dt, J = 5.5, 1.3 Hz, $1H_{A6}$), 8.36 (dt, J = 5.5, 1.6 Hz, $1H_{B6}$), 8.26 (d, J = 8.5 Hz, $1H_{B3}$), 8.08 (dd, J = 2.7, 1.0 Hz, $1H_{F5}$), 7.89 (d, J = 8.4 Hz, $1H_{A3}$), 7.82 (td, J = 8.5, 1.6 Hz, $1H_{B4}$), 7.76 (ddd, J = 8.4, 7.6, 1.3 Hz, $1H_{A4}$), 7.39 (dd, J = 9.2, 2.7 Hz, $1H_{F3}$), 7.25−7.21 (m, $2H_{A5,\ B5}$), 6.74 (d, J = 9.2 Hz, $1H_{F2}$), 6.45−6.39 (m, $2H_{C4,\ D4}$), 5.80 (dd, J = 8.6, 2.3 Hz, $1H_{C6}$), 5.51 (dd, J = 10.5, 5.7 Hz, $1H_{E4}$), 5.27 (dd, J = 8.8, 2.4 Hz, $1H_{D6}$), 4.86 (dd, J = 10.5, 9.4 Hz, $1H_{E5}$), 4.29 (dd, J = 9.4, 5.7 Hz, $1H_{E5}$); ^{19}F{^{1}H} NMR (376 MHz, d_2-1,1,2,2-TCE) δ (ppm) −60.34 (s, $3F_{CF3}$), −107.03 (d, J = 10.5 Hz, $1F_{dfppy}$), −107.63 (d, J = 9.9 Hz, $1F_{dfppy}$), −109.80 (d, J = 10.0 Hz, $1F_{dfppy}$), −110.36 (dd, J = 10.5, 2.8 Hz, $1F_{dfppy}$), −141.73 (dd, J = 22.6, 7.5 Hz, $1F_{G2/G6}$), −142.44 (dd, J = 22.2, 7.7 Hz, $1F_{G2/G6}$), −152.55 (t, J = 21.0 Hz, $1F_{G4}$), −159.59 (td, J = 21.0, 7.5 Hz, $1F_{G3/G5}$), −160.76 (td, J = 21.0, 7.5 Hz, $1F_{G3/G5}$); ^{13}C NMR (151 MHz, d_2-1,1,2,2-TCE) δ (ppm) 171.4 (C_{F1}), 165.5 (d, J = 9 Hz, C_{B2}), 164.4 (d, J = 263 Hz, C_{D5}), 165.0−160.0 ($C_{Ring\ G}$), 164.2 (d, J = 258 Hz, C_{C5}), 164.1 (d, J = 7 Hz, C_{A2}), 163.82 (C_{F6}), 161.6 (t, J = 273 Hz, C_{C3}), 161.6 (t, J = 273 Hz, C_{D3}), 155.5 (d, J = 6.0 Hz, C_{D1}), 150.5 (d, J = 7.1 Hz, C_{C1}), 148.7 (C_{A6}), 147.56 (C_{B6}), 138.30 (C_{B5}), 137.9 (C_{A4}), 130.1 (C_{F3}), 128.8 (C_{F5}), 128.4 (C_{D2}), 128.3 (C_{C2}), 125.8 (C_{F2}), 123.4 (d, J = 20.4 Hz, C_{B3}), 122.6 (C_{B5}), 122.2 (C_{A5}), 121.9 (d, J = 19.5 Hz, C_{A3}), 115.0 (d, J = 14.7 Hz, C_{C6}), 114.9 (C_{CF3}), 113.5 (C_{E2}), 113.3 (d, J = 15.9 Hz, C_{D6}), 108.7 (C_{F4}), 98.1 (t, J = 26.5 Hz, C_{D4}), 97.4 (t, J = 26.9 Hz, C_{C4}), 72.4 (C_{E5}), 61.3 (C_{E4}); HRMS (ESI) m/z 968.0905 [MH^+], calcd for $C_{38}H_{19}F_{12}IrN_3O_2^+$ 968.0892. Anal. Calcd for $C_{38}H_{18}F_{12}IrN_3O_2$: C, 47.11; H, 1.87; N, 4.34. Found: C, 46.98; H, 1.97; N, 4.26. Due to extensive coupling to ^{19}F nuclei, the ^{13}C signals for ring G are stated as a range. Crystals for X-ray analysis were grown by slow diffusion of *n*-hexane into a DCM solution of **1a**.

DOI: 10.1021/acs.inorgchem.8b02034
Inorg. Chem. XXXX, XXX, XXX−XXX

Complex ***1b***.

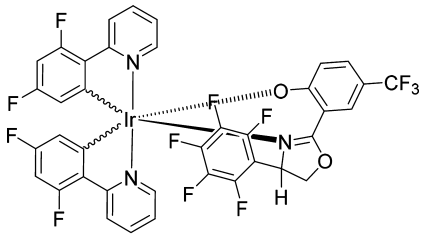

1b

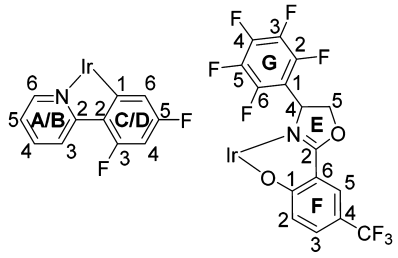

Isolated as an amorphous yellow powder (151 mg, 0.16 mmol, 30%): ^{1}H NMR (600 MHz, d_2-1,1,2,2-TCE) δ (ppm) 8.96 (ddd, J = 5.8, 1.6, 0.7 Hz, 1H$_{A6}$), 8.52 (dt, J = 5.6, 1.3 Hz, 1H$_{B6}$), 8.36 (d, J = 8.5 Hz, 1H$_{A3}$), 8.16 (d, J = 7.4 Hz, 1H$_{B3}$), 7.98−7.93 (m, 2H$_{A4,\ F5}$), 7.73 (td, J = 7.4, 1.3 Hz, 1H$_{B4}$), 7.35−7.29 (m, 2H$_{A5,\ F3}$), 7.04 (ddd, J = 7.4, 5.6, 1.4 Hz, 1H$_{B5}$), 6.56 (d, J = 9.0 Hz, 1H$_{F2}$), 6.41 (ddd, J = 12.0, 9.2, 2.4 Hz, 1H$_{C4}$), 6.32 (ddd, J = 12.0, 9.3, 2.4 Hz, 1H$_{D4}$), 5.47 (dd, J = 8.7, 2.4 Hz, 1H$_{C6}$), 5.19 (dd, J = 8.6, 2.4 Hz, 1H$_{D6}$), 4.63−4.54 (m, 2H$_{E4,\ E5}$), 4.36−4.29 (m, 1H$_{E5}$); ^{19}F{^{1}H} NMR (376 MHz, d_2-1,1,2,2-TCE) δ (ppm) −60.36 (s, 3F$_{CF3}$), −107.94 (d, J = 9.7 Hz, 1F$_{dfppy}$), −108.78 (d, J = 10.2 Hz, 1F$_{dfppy}$), −109.21 (d, J = 10.3 Hz, 1F$_{dfppy}$), −109.98 (d, J = 9.8 Hz, 1F$_{dfppy}$), −140.59 (d, J = 22.5 Hz, 1F$_{G2/G6}$), −142.17 (d, J = 22.5 Hz, 1F$_{G2/G6}$), −152.11 (t, J = 20.9 Hz, 1F$_{G4}$), −159.31 (t, J = 19.5 Hz, 1F$_{G3/G5}$), −161.08 (t, J = 22.1 Hz, 1F$_{G3/G5}$); ^{13}C NMR (151 MHz, d_2-1,1,2,2-TCE) δ (ppm) = 172.50 (C$_{F1}$), 165.0−160.0 (C$_{Ring\ G}$), 164.9 (C$_{A2}$), 164.7 (C$_{B2}$), 164.2 (C$_{F6}$), 162.4 (d, J = 259 Hz, C$_{D5}$), 162.3 (d, J = 249 Hz, C$_{C5}$), 161.2 (d, J = 261 Hz, C$_{D3}$), 160.6 Hz (d, J = 259 Hz, C$_{C3}$), 154.2 (d, J = 6.2 Hz, C$_{C1}$), 151.4 (d, J = 7.5 Hz, C$_{D1)}$, 149.6 (C$_{B6}$), 149.0 (C$_{A6}$), 138.8 (C$_{A4}$), 138.3 (C$_{B4}$), 130.4 (C$_{F3}$), 128.6 (C$_{C2}$), 128.4 (C$_{D2}$), 128.0 (C$_{F5}$), 124.9 (C$_{F2}$), 122.9 (C$_{B3}$), 122.8 (C$_{A3}$), 122.5 (C$_{A5}$), 121.8 (C$_{B5}$), 115.3 (C$_{CF3}$), 114.0 (d, J = 15.7 Hz, C$_{D6}$), 113.5 (d, J = 16.5 Hz, C$_{C6}$), 113.1 (C$_{E2}$), 110.7 (C$_{F4}$), 97.9 (t, J = 25.9 Hz, C$_{C4}$), 96.8 (t, J = 27.9 Hz, C$_{D4}$), 71.5 (C$_{E5}$), 59.7 (C$_{E4}$); HRMS (ESI) m/z 968.0919 [MH$^+$], calcd for $C_{38}H_{19}F_{12}IrN_3O_2^+$ 968.0892. Anal. Calcd for $C_{38}H_{18}F_{12}IrN_3O_2$: C, 47.11; H, 1.87; N, 4.34. Calcd for $C_{38}H_{18}F_{12}IrN_3O_2{\cdot}0.6CH_2Cl_2$: C, 45.46; H, 1.90; N, 4.12. Found: C, 45.30; H, 1.84; N, 4.11. Due to extensive coupling to ^{19}F nuclei, the ^{13}C signals for ring G are stated as a range. Crystals for X-ray analysis were grown by slow diffusion of *n*-hexane into a DCM solution of **1a**.

■ ASSOCIATED CONTENT

Supporting Information

The Supporting Information is available free of charge on the ACS Publications website at DOI: 10.1021/acs.inorgchem.8b02034.

NMR spectra, cyclic voltammograms, thermogravimetric analysis, and PhOLED data (PDF)

Computational atomic coordinates for **1a** (XYZ)

Computational atomic coordinates for **1b** (XYZ)

Accession Codes

CCDC 1850087−1850088 contain the supplementary crystallographic data for this paper. These data can be obtained free of charge via www.ccdc.cam.ac.uk/data_request/cif, or by emailing data_request@ccdc.cam.ac.uk, or by contacting The Cambridge Crystallographic Data Centre, 12 Union Road, Cambridge CB2 1EZ, UK; fax: +44 1223 336033.

■ AUTHOR INFORMATION

Corresponding Authors

*E-mail for Y.L.: yuliu@jlu.edu.cn.

*E-mail for D.Z.: zhudx047@nenu.edu.cn.

*E-mail for M.R.B.: m.r.bryce@durham.ac.uk.

ORCID

Andrei S. Batsanov: 0000-0002-4912-0981

Yu Liu: 0000-0001-8686-1503

Martin R. Bryce: 0000-0003-2097-7823

Notes

The authors declare no competing financial interest.

■ ACKNOWLEDGMENTS

Dr. Alan Kenwright and Dr. Juan Aguilar-Malavia are acknowledged for their help with the variable-temperature NMR experiments. Prof. Andrew Beeby is acknowledged for his help with the variable-temperature PL experiments. We thank the EPSRC for funding the work in Durham (grant EP/L02621X/1). The NSFC (Nos. 51773078, 51473028), the key scientific and technological project of Jilin province (20160307016GX), and the development and reform commission of Jilin province (20160058) are thanked for funding the work in China.

■ REFERENCES

(1) Chen, Z. Q.; Bian, Z. Q.; Huang, C. H. Functional Ir(III) Complexes and Their Applications. *Adv. Mater.* **2010**, *22*, 1534−1539.

(2) *Iridium(III) in Optoelectronic and Photonics Applications*; Zysman-Colman, E., Ed.; Wiley: 2017.

(3) Lowry, M. S.; Bernhard, S. Synthetically Tailored Excited States: Phosphorescent, Cyclometalated Iridium(III) Complexes and Their Applications. *Chem. - Eur. J.* **2006**, *12*, 7970−7977.

(4) Lo, K. K.-W.; Tsang, K. H.-K.; Sze, K.-S.; Chung, C.-K.; Lee, T. K.-M.; Zhang, K. Y.; Hui, W.-K.; Li, C.-K.; Lau, J. S.-Y.; Ng, D. C.-M.; et al. Non-Covalent Binding of Luminescent Transition Metal Polypyridine Complexes to Avidin, Indole-Binding Proteins and Estrogen Receptors. *Coord. Chem. Rev.* **2007**, *251*, 2292−2310.

(5) Gao, R.; Ho, D. G.; Hernandez, B.; Selke, M.; Murphy, D.; Djurovich, P. I.; Thompson, M. E. Bis-Cyclometalated Ir(III) Complexes as Efficient Singlet Oxygen Sensitizers. *J. Am. Chem. Soc.* **2002**, *124*, 14828−14829.

(6) Yang, X.; Zhou, G.; Wong, W.-Y. Functionalization of Phosphorescent Emitters and Their Host Materials by Main-Group Elements for Phosphorescent Organic Light-Emitting Devices. *Chem. Soc. Rev.* **2015**, *44*, 8484−8575.

(7) Ulbricht, C.; Beyer, B.; Friebe, C.; Winter, A.; Schubert, U. S. Recent Developments in the Application of Phosphorescent Iridium(III) Complex Systems. *Adv. Mater.* **2009**, *21*, 4418−4441.

(8) Kwon, Y.; Han, S. H.; Yu, S.; Lee, J. Y.; Lee, K. M. Functionalized Phenylimidazole-Based Facial-Homoleptic Iridium(III) Complexes and Their Excellent Performance in Blue Phosphorescent Organic Light-Emitting Diodes. *J. Mater. Chem. C* **2018**, *6*, 4565−4572.

(9) Zhang, D.; Qiao, J.; Zhang, D.; Duan, L. Ultrahigh-Efficiency Green PHOLEDs with a Voltage under 3 V and a Power Efficiency of Nearly 110 Lm W^{-1} at Luminance of 10 000 cd m^{-2}. *Adv. Mater.* **2017**, *29*, 1702847.

(10) Udagawa, K.; Sasabe, H.; Igarashi, F.; Kido, J. Simultaneous Realization of High EQE of 30%, Low Drive Voltage, and Low Efficiency Roll-Off at High Brightness in Blue Phosphorescent OLEDs. *Adv. Opt. Mater.* **2016**, *4*, 86−90.

DOI: 10.1021/acs.inorgchem.8b02034
Inorg. Chem. XXXX, XXX, XXX−XXX

(11) Li, C.; Fan, X.; Han, C.; Xu, H. A Ternary Phosphine Oxide Host Featuring Thermally Activated Delayed Fluorescence for Blue PHOLEDs with > 20% EQE and Extremely Low Roll-Offs. *J. Mater. Chem. C* **2018**, *6*, 6747−6754.
(12) Miao, Y.; Tao, P.; Gao, L.; Li, X.; Wei, L.; Liu, S.; Wang, H.; Xu, B.; Zhao, Q. Highly Efficient Chlorine Functionalized Blue Iridium(III) Phosphors for Blue and White Phosphorescent Organic Light-Emitting Diodes with the External Quantum Efficiency Exceeding 20%. *J. Mater. Chem. C* **2018**, *6*, 6656−6665.
(13) Chi, Y.; Chou, P.-T. Transition-Metal Phosphors with Cyclometalating Ligands: Fundamentals and Applications. *Chem. Soc. Rev.* **2010**, *39*, 638−655.
(14) Ladouceur, S.; Zysman-Colman, E. Iridium Complexes A Comprehensive Survey of Cationic Iridium(III) Complexes Bearing Nontraditional Ligand Chelation Motifs. *Eur. J. Inorg. Chem.* **2013**, *2013*, 2985−3007.
(15) Henwood, A. F.; Zysman-Colman, E. Lessons Learned in Tuning the Optoelectronic Properties of Phosphorescent Iridium(III) Complexes. *Chem. Commun.* **2017**, *53*, 807−826.
(16) Benjamin, H.; Zheng, Y.; Batsanov, A. S.; Fox, M. A.; Al-Attar, H. A.; Monkman, A. P.; Bryce, M. R. Sulfonyl-Substituted Heteroleptic Cyclometalated Iridium(III) Complexes as Blue Emitters for Solution-Processable Phosphorescent Organic Light-Emitting Diodes. *Inorg. Chem.* **2016**, *55*, 8612−8627.
(17) Yang, X.; Sun, N.; Dang, J.; Huang, Z.; Yao, C.; Xu, X.; Ho, C.-L.; Zhou, G.; Ma, D.; Zhao, X.; et al. Versatile Phosphorescent Color Tuning of Highly Efficient Borylated Iridium(III) Cyclometalates by Manipulating the Electron-Accepting Capacity of the Dimesitylboron Group. *J. Mater. Chem. C* **2013**, *1*, 3317−3326.
(18) Baranoff, E.; Curchod, B. F. E.; Frey, J.; Scopelliti, R.; Kessler, F.; Tavernelli, I.; Rothlisberger, U.; Gra, M.; Nazeeruddin, K. Acid-Induced Degradation of Phosphorescent Dopants for OLEDs and Its Application to the Synthesis of Tris-Heteroleptic Iridium(III) Bis-Cyclometalated Complexes. *Inorg. Chem.* **2012**, *51*, 215−224.
(19) Baranoff, E.; Jung, I.; Scopelliti, R.; Solari, E.; Grätzel, M.; Nazeeruddin, M. K. Room-Temperature Combinatorial Screening of Cyclometallated Iridium(III) Complexes for a Step towards Molecular Control of Colour Purity. *Dalton Trans* **2011**, *40*, 6860−6867.
(20) Rausch, A. F.; Thompson, M. E.; Yersin, H. Blue Light Emitting Ir(III) Compounds for OLEDs - New Insights into Ancillary Ligand Effects on the Emitting Triplet State. *J. Phys. Chem. A* **2009**, *113*, 5927−5932.
(21) Li, J.; Djurovich, P. I.; Alleyne, B. D.; Yousufuddin, M.; Ho, N. N.; Thomas, J. C.; Peters, J. C.; Bau, R.; Thompson, M. E. Synthetic Control of Excited-State Properties in Cyclometalated Ir(III) Complexes Using Ancillary Ligands. *Inorg. Chem.* **2005**, *44*, 1713−1727.
(22) Gu, X.; Fei, T.; Zhang, H.; Xu, H.; Yang, B.; Ma, Y.; Liu, X. Tuning the Emission Color of Iridium(III) Complexes with Ancillary Ligands: A Combined Experimental and Theoretical Study. *Eur. J. Inorg. Chem.* **2009**, *2009*, 2407−2414.
(23) Chiu, Y.-C.; Chi, Y.; Hung, J.-Y.; Cheng, Y.-M.; Yu, Y.-C.; Chung, M.-W.; Lee, G.-H.; Chou, P.-T.; Chen, C.-C.; Wu, C.-C.; et al. Blue to True-Blue Phosphorescent Ir(III) Complexes Bearing a Nonconjugated Ancillary Phosphine Chelate: Strategic Synthesis, Photophysics, and Device Integration. *ACS Appl. Mater. Interfaces* **2009**, *1*, 433−442.
(24) Kim, T.; Lee, J.; Lee, S. U.; Lee, M. H. *O* -Carboranyl−Phosphine as a New Class of Strong-Field Ancillary Ligand in Cyclometalated Iridium(III) Complexes: Toward Blue Phosphorescence. *Organometallics* **2015**, *34*, 3455−3458.
(25) Henwood, A. F.; Evariste, S.; Slawin, A. M. Z.; Zysman-Colman, E. Rigid Biimidazole Ancillary Ligands as an Avenue to Bright Deep Blue Cationic iridium(III) Complexes. *Faraday Discuss.* **2014**, *174*, 165−182.
(26) Benjamin, H.; Fox, M. A.; Batsanov, A. S.; Al-Attar, H. A.; Li, C.; Ren, Z.; Monkman, A. P.; Bryce, M. R. Pyridylpyrazole N̂N Ligands Combined with Sulfonyl-Functionalised Cyclometalating Ligands for Blue-Emitting I Iridium(III) Complexes and Solution-Processable PhOLEDs. *Dalton Trans* **2017**, *46*, 10996−11007.
(27) You, Y.; Seo, J.; Kim, S. H.; Kim, K. S.; Ahn, T. K.; Kim, D.; Park, S. Y. Highly Phosphorescent Iridium Complexes with Chromophoric 2-(2-Hydroxyphenyl)oxazole-Based Ancillary Ligands: Interligand Energy-Harvesting Phosphorescence. *Inorg. Chem.* **2008**, *47*, 1476−1487.
(28) Chao, K.; Shao, K.; Peng, T.; Zhu, D.; Wang, Y.; Liu, Y.; Su, Z.; Bryce, M. R. New Oxazoline- and Thiazoline-Containing Heteroleptic Iridium(III) Complexes for Highly-Efficient Phosphorescent Organic Light-Emitting Devices (PhOLEDs): Colour Tuning by Varying the Electroluminescence Bandwidth. *J. Mater. Chem. C* **2013**, *1*, 6800−6806.
(29) Benjamin, H.; Liang, J.; Liu, Y.; Geng, Y.; Liu, X.; Zhu, D.; Batsanov, A. S.; Bryce, M. R. Color Tuning of Efficient Electroluminescence in the Blue and Green Regions Using Heteroleptic Iridium Complexes with 2-Phenoxyoxazole Ancillary Ligands. *Organometallics* **2017**, *36*, 1810−1821.
(30) Marchi, E.; Sinisi, R.; Bergamini, G.; Tragni, M.; Monari, M.; Bandini, M.; Ceroni, P. Easy Separation of Δ and Λ Isomers of Highly Luminescent [Ir(III)]-Cyclometalated Complexes Based on Chiral Phenol-Oxazoline Ancillary Ligands. *Chem. - Eur. J.* **2012**, *18*, 8765−8773.
(31) Yi, S.; Kim, J. H.; Cho, Y. J.; Lee, J.; Choi, T. S.; Cho, D. W.; Pac, C.; Han, W. S.; Son, H. J.; Kang, S. O. Stable Blue Phosphorescence Iridium(III) Cyclometalated Complexes Prompted by Intramolecular Hydrogen Bond in Ancillary Ligand. *Inorg. Chem.* **2016**, *55*, 3324−3331.
(32) Li, L. P.; Yao, S. Y.; Ou, Y. L.; Wei, L. Q.; Ye, B. H. Diastereoselective Synthesis and Photophysical Properties of Bis-Cyclometalated Ir(III) Stereoisomers with Dual Stereocenters. *Organometallics* **2017**, *36*, 3257−3265.
(33) Bünzli, A. M.; Constable, E. C.; Housecroft, C. E.; Prescimone, A.; Zampese, J. A.; Longo, G.; Gil-Escrig, L.; Pertegás, A.; Ortí, E.; Bolink, H. J. Exceptionally Long-Lived Light-Emitting Electrochemical Cells: Multiple Intra-Cation π-Stacking Interactions in [Ir(ĈN)2(N̂N)][PF6] Emitters. *Chem. Sci.* **2015**, *6*, 2843−2852.
(34) Constable, E. C.; Housecroft, C. E.; Kopecky, P.; Martin, C. J.; Wright, I. A.; Zampese, J. A.; Bolink, H. J.; Pertegas, A. Solution, Structural and Photophysical Aspects of Substituent Effects in the N̂N Ligand in [Ir(ĈN)2(N̂N)]+ Complexes. *Dalton Trans* **2013**, *42*, 8086−8103.
(35) He, L.; Ma, D.; Duan, L.; Wei, Y.; Qiao, J.; Zhang, D.; Dong, G.; Wang, L.; Qiu, Y. Control of Intramolecular π-π Stacking Interaction in Cationic Iridium Complexes via Fluorination of Pendant Phenyl Rings. *Inorg. Chem.* **2012**, *51*, 4502−4510.
(36) Kumar, S.; Hisamatsu, Y.; Tamaki, Y.; Ishitani, O.; Aoki, S. Design and Synthesis of Heteroleptic Cyclometalated Iridium(III) Complexes Containing Quinoline-Type Ligands That Exhibit Dual Phosphorescence. *Inorg. Chem.* **2016**, *55*, 3829−3843.
(37) Li, P.; Shan, G. G.; Cao, H. T.; Zhu, D. X.; Su, Z. M.; Jitchati, R.; Bryce, M. R. Intramolecular π Stacking in Cationic Iridium(III) Complexes with Phenyl-Functionalized Cyclometalated Ligands: Synthesis, Structure, Photophysical Properties, and Theoretical Studies. *Eur. J. Inorg. Chem.* **2014**, *2014*, 2376−2382.
(38) Congrave, D. G.; Hsu, Y.-T.; Batsanov, A. S.; Beeby, A.; Bryce, M. R. Sky-Blue Emitting Bridged Diiridium Complexes: Beneficial Effects of Intramolecular π−π Stacking. *Dalton Trans* **2018**, *47*, 2086−2098.
(39) Cockroft, S. L.; Hunter, C. A.; Lawson, K. R.; Perkins, J.; Urch, C. J. Electrostatic Control of Aromatic Stacking Interactions. *J. Am. Chem. Soc.* **2005**, *127*, 8594−8595.
(40) Cozzi, F.; Cinquini, M.; Annuziata, R.; Siegel, J. S. Dominance of Polar/pi over Charge-Transfer Effects in Stacked Phenyl Interactions. *J. Am. Chem. Soc.* **1993**, *115*, 5330−5331.
(41) Cozzi, F.; Ponzini, F.; Annunziata, R.; Cinquini, M.; Siegel, J. S. Polar Interactions between Stacked Pi Systems in Fluorinated 1,8-Diarylnaphthalenes: Importance of Quadrupole Moments in Molecular Recognition. *Angew. Chem., Int. Ed. Engl.* **1995**, *34*, 1019−1020.

DOI: 10.1021/acs.inorgchem.8b02034
Inorg. Chem. XXXX, XXX, XXX−XXX

(42) Cockroft, S. L.; Hunter, C. A. Chemical Double-Mutant Cycles : Dissecting Non-Covalent Interactions. *Chem. Soc. Rev.* **2007**, *36*, 172−188.
(43) Camara-Campos, A.; Musumeci, D.; Hunter, C. A.; Turega, S. Chemical Double Mutant Cycles for the Quantification of Cooperativity in H-Bonded Complexes. *J. Am. Chem. Soc.* **2009**, *131*, 18518−18524.
(44) Adams, H.; Carver, F. J.; Hunter, C. A.; Morales, J. C.; Seward, E. M. Chemical Double-Mutant Cycles for the Measurement of Weak Intermolecular Interactions: Edge-to-Face Aromatic Interactions. *Angew. Chem., Int. Ed. Engl.* **1996**, *35*, 1542−1544.
(45) Li, T.-Y.; Zheng, Y.-X.; Zhou, Y.-H. Iridium(III) Phosphorescent Complexes with Dual Stereogenic Centers: Single Crystal, Electronic Circular Dichroism Evidence and Circularly Polarized Luminescence Properties. *Dalton Trans* **2016**, *45*, 19234−19237.
(46) Bandini, M.; Cozzi, P. G.; Gazzano, M.; Umani-Ronchi, A. An Effective and Useful Synthesis of Enantiomerically Enriched Arylglycinols. *Eur. J. Org. Chem.* **2001**, *2001*, 1937−1942.
(47) Wang, J.; Luis, J.; Pozo, C.; Sorochinsky, A. E.; Fustero, S.; Soloshonok, V. A.; Liu, H. Fluorine in Pharmaceutical Industry : Fluorine-Containing Drugs Introduced to the Market in the Last Decade (2001 − 2011). *Chem. Rev.* **2014**, *114*, 2432−2506.
(48) Martir, D. R.; Momblona, C.; Pertegás, A.; Cordes, D. B.; Slawin, A. M. Z.; Bolink, H. J.; Zysman-Colman, E. Chiral Iridium(III) Complexes in Light-Emitting Electrochemical Cells: Exploring the Impact of Stereochemistry on the Photophysical Properties and Device Performances. *ACS Appl. Mater. Interfaces* **2016**, *8*, 33907−33915.
(49) Cudre, Y.; de Carvalho, F. F.; Burgess, G. R.; Male, L.; Pope, S. J. A.; Tavernelli, I.; Baranoff, E. Tris-Heteroleptic Iridium Complexes Based on Cyclometalated Ligands with Different Cores. *Inorg. Chem.* **2017**, *56*, 11565−11576.
(50) Feldman, J.; Vo, G. D.; McLaren, C. D.; Gehret, T. C.; Park, K. H.; Meth, J. S.; Marshall, W. J.; Buriak, J.; Bryman, L. M.; Dobbs, K. D.; et al. Highly Quantum Efficient Phosphorescent Sky Blue Emitters Based on Diastereomeric Iridium(III) Complexes of Atropisomeric 5-Aryl-4H-1,2,4-Triazole Ligands. *Organometallics* **2015**, *34*, 3665−3669.
(51) Dolomanov, O. V.; Bourhis, L. J.; Gildea, R. J.; Howard, J. A. K.; Puschmann, H. OLEX2: A Complete Structure Solution, Refinement and Analysis Program. *J. Appl. Crystallogr.* **2009**, *42*, 339−341.
(52) Berger, S.; Braun, S.; Kalinowski, H.-O. *NMR Spectroscopy of the Non-Metallic Elements*, 1st ed.; Wiley: 1997.
(53) Banks, R. E.; Haszeldine, R. N. Heterocyclic Polyfluoro-Compounds. Part X. Nucleophilic Substitution in Tetrafluoropyrimidine. *J. Chem. Soc. C* **1967**, 1822−1826.
(54) Klauke, E.; Oehlmann, L.; Baasner, B. Fluorinated Heterocyclic Compounds: Selective Chlorine/ Fluorine Exchange Reactions on Pyrimidines. *J. Fluorine Chem.* **1982**, *21*, 495−513.
(55) Zhou, J.; Kuntze-Fechner, M. W.; Bertermann, R.; Paul, U. S. D.; Berthel, J. H. J.; Friedrich, A.; Du, Z.; Marder, T. B.; Radius, U. Preparing (Multi)Fluoroarenes as Building Blocks for Synthesis: Nickel-Catalyzed Borylation of Polyfluoroarenes via C-F Bond Cleavage. *J. Am. Chem. Soc.* **2016**, *138*, 5250−5253.
(56) Abraham, R. J.; Macdonald, D. B.; Pepper, E. S. The Nuclear Magnetic Resonance Spectra of Fluorobenzenes. II. The Effect of Substituents on the Meta and Para Fluorine-Fluorine Coupling Constants. *J. Am. Chem. Soc.* **1968**, *90*, 147−153.
(57) Günther, H. *NMR Spectroscopy: Basic Principles, Concepts and Applications in Chemistry*, 2nd ed.; Wiley: Chichester, U.K., 1995.
(58) Congrave, D. G.; Hsu, Y.; Batsanov, A. S.; Beeby, A.; Bryce, M. R. Synthesis, Diastereomer Separation, and Optoelectronic and Structural Properties of Dinuclear Cyclometalated Iridium(III) Complexes with Bridging Diarylhydrazide Ligands. *Organometallics* **2017**, *36*, 981−993.
(59) Yang, X.; Xu, X.; Dang, J.; Zhou, G.; Ho, C.-L.; Wong, W.-Y. From Mononuclear to Dinuclear Iridium(III) Complex: Effective Tuning of the Optoelectronic Characteristics for Organic Light-Emitting Diodes. *Inorg. Chem.* **2016**, *55*, 1720−1727.
(60) Frey, J.; Curchod, B. F. E.; Scopelliti, R.; Tavernelli, I.; Rothlisberger, U.; Nazeeruddin, M. K.; Baranoff, E. Structure-Property Relationships Based on Hammett Constants in Cyclometalated iridium(III) Complexes: Their Application to the Design of a Fluorine-Free FIrPic-like Emitter. *Dalton Trans* **2014**, *43*, 5667−5679.
(61) Tamayo, A. B.; Alleyne, B. D.; Djurovich, P. I.; Lamansky, S.; Tsyba, I.; Ho, N. N.; Bau, R.; Thompson, M. E. Synthesis and Characterization of Facial and Meridional Tris-Cyclometalated iridium(III) Complexes. *J. Am. Chem. Soc.* **2003**, *125*, 7377−7387.
(62) Sajoto, T.; Djurovich, P. I.; Tamayo, A.; Yousufuddin, M.; Bau, R.; Thompson, M. E.; Holmes, R. J.; Forrest, S. R. Blue and near-UV Phosphorescence from Iridium Complexes with Cyclometalated Pyrazolyl or N-Heterocyclic Carbene Ligands. *Inorg. Chem.* **2005**, *44*, 7992−8003.
(63) Sajoto, T.; Djurovich, P. I.; Tamayo, A. B.; Oxgaard, J.; Goddard, W. A.; Thompson, M. E. Temperature Dependence of Blue Phosphorescent Cyclometalated Ir(III) Complexes. *J. Am. Chem. Soc.* **2009**, *131*, 9813−9822.
(64) Mao, H. T.; Zang, C. X.; Wen, L. L.; Shan, G. G.; Sun, H. Z.; Xie, W. F.; Su, Z. M. Ir(III) Phosphors Modified with Fluorine Atoms in Pyridine-1,2,4-Triazolyl Ligands for Efficient OLEDs Possessing Low-Efficiency Roll-Off. *Organometallics* **2016**, *35*, 3870−3877.
(65) Sivasubramaniam, V.; Brodkorb, F.; Hanning, S.; Loebl, H. P.; van Elsbergen, V.; Boerner, H.; Scherf, U.; Kreyenschmidt, M. Fluorine Cleavage of the Light Blue Heteroleptic Triplet Emitter FIrpic. *J. Fluorine Chem.* **2009**, *130*, 640−649.
(66) Tordera, D.; Delgado, M.; Orti, E.; Bolink, H. J.; Frey, J.; Nazeeruddin, M. K.; Baranoff, E. Stable Green Electroluminescence from an Iridium Tris-Heteroleptic Ionic Complex. *Chem. Mater.* **2012**, *24*, 1896−1903.
(67) Tordera, D.; Serrano-Perez, J. J.; Pertegas, A.; Orti, E.; Bolink, H. J.; Baranoff, E.; Nazeeruddin, M. K.; Frey, J. Correlating the Lifetime and Fluorine Content of Iridium(III) Emitters in Green Light-Emitting Electrochemical Cells. *Chem. Mater.* **2013**, *25*, 3391−3397.
(68) Baranoff, E.; Curchod, B. F. E. FIrpic: Archetypal Blue Phosphorescent Emitter for Electroluminescence. *Dalton Trans* **2015**, *44*, 8318−8329.
(69) Frisch, M. J.; Trucks, G. W.; Schlegel, H. B.; Scuseria, G. E.; Robb, M. A.; Cheeseman, J. R.; Scalmani, G.; Barone, V.; Mennucci, B.; Petersson, G. A.; Nakatsuji, H.; Caricato, M.; Li, X.; Hratchian, H. P.; Izmaylov, A. F.; Bloino, J.; Zheng, G.; Sonnenber, D. J. *Gaussian 09*; Gaussian, Inc., Wallingford, CT, 2009; 2−3.
(70) Becke, A. D. Density-Functional Thermochemistry. III. The Role of Exact Exchange. *J. Chem. Phys.* **1993**, *98*, 5648.
(71) Lee, C.; Yang, W.; Parr, R. G. Development of the Colle-Salvetti Correlation-Energy Formula into a Functional of the Electron Density. *Phys. Rev. B: Condens. Matter Mater. Phys.* **1988**, *37*, 785−789.
(72) Hay, P. J.; Wadt, W. R. Ab Initio Effective Core Potentials for Molecular Calculations. Potentials for the Transition Metal Atoms Sc to Hg. *J. Chem. Phys.* **1985**, *82*, 270−283.
(73) Wadt, W. R.; Hay, P. J. Ab Initio Effective Core Potentials for Molecular Calculations. Potentials for Main Group Elements Na to Bi. *J. Chem. Phys.* **1985**, *82*, 284−298.
(74) Hay, P. J.; Wadt, W. R. Ab Initio Effective Core Potentials for Molecular Calculations. Potentials for K to Au Including the Outermost Core Orbitals. *J. Chem. Phys.* **1985**, *82*, 299−310.
(75) Petersson, G. A.; Bennett, A.; Tensfeldt, T. G.; Al-Laham, M. A.; Shirley, W. A.; Mantzaris, J. A Complete Basis Set Model Chemistry. II. Open-Shell Systems and the Total Energies of the First-Row Atoms. *J. Chem. Phys.* **1991**, *94*, 6081−6090.
(76) Petersson, G. A.; et al. A Complete Basis Set Model Chemistry. I. The Total Energies of Closed-Shell Atoms and Hydrides of the First-Row Elements. *J. Chem. Phys.* **1988**, *89*, 2193−2218.

DOI: 10.1021/acs.inorgchem.8b02034
Inorg. Chem. XXXX, XXX, XXX−XXX

(77) Allouche, A.-R. Gabedit: A Graphical User Interface For Computational Chemistry Softwares. *J. Comput. Chem.* **2011**, *32*, 174−182.
(78) O'Boyle, N. M.; Tenderholt, A. L.; Langner, K. M. Cclib: A Library for Package-Independent Computational Chemistry Algorithms. *J. Comput. Chem.* **2008**, *29*, 839−845.
(79) Sheldrick, G. M. A Short History of SHELX. *Acta Crystallogr., Sect. A: Found. Crystallogr.* **2008**, *64*, 112−122.
(80) Sheldrick, G. M. Crystal Structure Refinement With SHELXL. *Acta Crystallogr., Sect. C: Struct. Chem.* **2015**, *71*, 3−8.
(81) Pålsson, B. L.; Monkman, A. P. Measurements of Solid-State Photoluminescence Quantum Yields of Films Using a Fluorimeter. *Adv. Mater.* **2002**, *14*, 757−758.
(82) Sprouse, S.; King, K. A.; Spellane, P. J.; Watts, R. J. Photophysical Effects of Metal-Carbon Bonds in Ortho-Metalated Complexes of Ir (III) and Rh (III). *J. Am. Chem. Soc.* **1984**, *106*, 6647−6653.

DOI: 10.1021/acs.inorgchem.8b02034
Inorg. Chem. XXXX, XXX, XXX−XXX